A *Ctnnb1* enhancer transcriptionally regulates Wnt signaling dosage to balance homeostasis and tumorigenesis of intestinal epithelia

Xiaojiao Hua[1,2], Chen Zhao[1,2], Jianbo Tian[4,5], Junbao Wang[1,2], Xiaoping Miao[4,5], Gen Zheng[6], Min Wu[2,3,5], Mei Ye[7], Ying Liu[1,2,*], Yan Zhou[1,2,*]

[1]Department of Neurosurgery, Medical Research Institute, Zhongnan Hospital of Wuhan University, Wuhan University, Wuhan, China

[2]Frontier Science Center of Immunology and Metabolism, Wuhan University, Wuhan, China

[3]College of Life Sciences, Wuhan University, Wuhan, China

[4]Department of Epidemiology and Biostatistics, School of Public Health, Wuhan University, Wuhan, China.

[5]TaiKang Center for Life and Medical Sciences, Wuhan University, Wuhan, China

[6]Department of Gastroenterology, Union Hospital, Tongji Medical College, Huazhong University of Science and Technology, Wuhan, China

[7]Department of Gastroenterology, Zhongnan Hospital of Wuhan University, Wuhan, China

*Correspondence to Dr. Ying Liu, y.liu@whu.edu.cn; Dr. Yan Zhou, yan.zhou@whu.edu.cn

Abstract

The β-catenin-dependent canonical Wnt signaling is pivotal in organ development, tissue homeostasis, and cancer. Here we identified an upstream enhancer of *Ctnnb1* – the coding gene for β-catenin, named ieCtnnb1 (intestinal enhancer of *Ctnnb1*), which is crucial for intestinal homeostasis. ieCtnnb1 is predominantly active in the base of small intestinal crypts and throughout the

epithelia of large intestine. Knockout of ieCtnnb1 led to a reduction in *Ctnnb1* transcription, compromising the canonical Wnt signaling in intestinal crypts. Single-cell sequencing revealed that ieCtnnb1 knockout altered epithelial compositions and potentially compromised functions of small intestinal crypts. While deletion of ieCtnnb1 hampered epithelial turnovers in physiologic conditions, it prevented occurrence and progression of Wnt/β-catenin-driven colorectal cancers. Human ieCTNNB1 drove reporter gene expression in a pattern highly similar to mouse ieCtnnb1. ieCTNNB1 contains a single-nucleotide polymorphism associated with *CTNNB1* expression levels in human gastrointestinal epithelia. The enhancer activity of ieCTNNB1 in colorectal cancer tissues was stronger than that in adjacent normal tissues. HNF4α and phosphorylated CREB1 were identified as key trans-factors binding to ieCTNNB1 and regulating *CTNNB1* transcription. Together, these findings unveil an enhancer-dependent mechanism controlling the dosage of Wnt signaling and homeostasis in intestinal epithelia.

Introduction

The gastrointestinal (GI) epithelium, a high turnover organ, contains multiple cell types to fulfill complex functions including food digestion, nutrient absorption, pathogen insulation and clearance, as well as endocrine roles (**Noah et al., 2011; Chin et al., 2017; Kurokawa et al., 2020**). Enterocytes (ECs) constitute ~90% of all differentiated cells and function as highly efficient cells for absorbing nutrients and water (**Snoeck et al., 2005**). Goblet cells (GCs) produce mucus to lubricate the mucosal surface (**Gustafsson & Johansson, 2022**). Enteroendocrine cells (EECs) sense luminal nutrients and secrete peptide hormones to regulate appetite, intestinal motility, and insulin release (**Gribble & Reimann, 2019**). Tuft cells (TCs) are chemosensory cells that respond to various stimuli including infections and hypoxia (**Schneider et al., 2019**). The crypts of GI epithelium harbor various types of stem cells that

58 continually replenish lost epithelial cells **(van der Flier & Clevers, 2009;**
59 **Ramadan et al., 2022**). While the prevailing belief is that *Lgr5*-expressing crypt
60 base columnar (CBC) cells are actively dividing stem cells and *Bmi*-expressing
61 " +4 " cells (positioned four cells above the base of the crypt) are slowly cycling
62 stem cells, it's important to note that crypt cells have the capacity for fate
63 reprogramming and de-differentiation to sustain regenerative capability (**Barker**
64 **et al., 2007; Tian et al., 2011; Yan et al., 2012; Metcalfe et al., 2014; Beumer**
65 **& Clevers, 2016**). Intestinal stem cells generate transit-amplifying cells (TACs),
66 which undergo multiple cell divisions and differentiate into all intestinal lineages
67 while migrating towards the crypt orifice (**Krausova & Korinek, 2014**). In
68 addition to stem and progenitor cells, the base of small intestinal crypts contains
69 Paneth cells (PCs) that secret antimicrobial peptides, called defensins, thereby
70 contributing to host defense against microbes (**Lueschow & McElroy, 2020;**
71 **Barreto et al., 2022**). PCs also contribute to the stem cell niche function, *e.g.*
72 secreting Wnt ligands, to maintain epithelial homeostasis of the small intestine
73 (**Sato et al., 2011**).
74 The behavior of crypt cells is precisely regulated by multiple signals, which
75 can act sequentially, additively, synergistically, or antagonistically (**Nakamura**
76 **et al., 2007**). Among them, the Wnt/β-catenin signal pathway represents the
77 principal force governing intestinal epithelium homeostasis, particularly in the
78 preservation of stem cell proliferation and multipotency **(Pinto et al., 2003;**
79 **Clevers et al., 2014; Mah et al., 2016**). Upon Wnt ligand binding, the β-catenin
80 degradation complex is inactivated, leading to accumulation of β-catenin and
81 its translocation into the nucleus, where it works with the co-activator TCF7L2
82 to turn on the transcription of a plethora of target genes, including *MYC*, *CCND1*,
83 *AXIN2*, and *CD44* (**Clevers, 2006; Clevers & Nusse, 2012; Nusse & Clevers,**
84 **2017**). Inhibition of Wnt ligand secretion reduced number of functional stem
85 cells and led to a faster crypt fixation rate (**Huels et al., 2018**). In the process
86 of aging, reduced Wnt signaling in stem cells and the niche of intestinal crypts

87 causes inhibition of proliferation and reduced numbers of intestinal stem cells
88 (**Nalapareddy et al., 2017; Pentinmikko et al., 2019**). The Wnt signal is also
89 essential for commitment, maturation, and location of PCs and other secretory
90 cells (**van Es et al., 2005; Andreu et al., 2008**). On the other hand, Wnt, EGF
91 and Delta-like 1/4 ligands presented by PCs sustained CBCs' proliferative
92 states and the production (**Sato et al., 2011**). Although the Wnt signal dosage,
93 largely *via* post-translational regulations, controls early lineage specification,
94 hematopoiesis, and tumorigenesis (**Luis et al., 2011; Bakker et al., 2013**), it
95 remains elusive how Wnt signaling dosage, particularly through the
96 transcriptional control of *Ctnnb1* – the coding gene for β-catenin, regulates
97 composition and function of intestinal epithelia.

98 Aberrant activation of canonical Wnt signaling is associated with GI cancers,
99 most notably colorectal cancer (CRC) (**Zhao et al., 2022; Zhu & Li, 2023**).
100 Germinal mutations of the *APC* gene, which encodes the negative regulator of
101 β-catenin, underlie the Familial Adenomatous Polyposis (FAP), a hereditary
102 neoplastic syndrome and the pre-cancerous condition for CRC (**Cheng et al.,**
103 **2019; J. Li et al., 2021**). Moreover, *APC* is mutated in up to 80% of human
104 sporadic CRCs (**J. Li et al., 2021**). Inactivation of APC causes enhanced
105 accumulation of β-catenin in nuclei and subsequent activation of proliferative
106 and pro-survival signals in CRC cells (**Cheng et al., 2019**). However, largely
107 due to lack of specificity, no molecular therapeutic strategy targeting the
108 pathway has been incorporated into CRC treatment. Interestingly, the
109 transcriptional activity of *CTNNB1*, the coding gene for β-catenin, is also
110 enhanced in CRCs (**Terrin et al., 2017**); however, the underlying mechanism is
111 largely unknown. Dissecting it would facilitate the development of new Wnt/β-
112 catenin targeting means to treat CRC.

113 Enhancers are essential *cis*-regulatory DNA elements that control
114 spatiotemporal gene expressions during cell fate specification and
115 maintenance (**Pachano et al., 2022**). Active enhancers are often associated

with cell fate specifiers, mostly transcription factors (TFs), and are enriched with specific histone modification such as H3K27ac (acetylated lysine 27 of histone H3) and H3K4me1 (mono-methylated lysine 4) of histone H3 (**Jindal & Farley, 2021**). Importantly, variations of enhancer sequences often lead to aberrant gene silence and activation, thereby causing developmental anomalies and cancers (**Zabidi & Stark, 2016; Sengupta & George, 2017; Kvon et al., 2021**). Although numerous putative enhancers have been identified by high-throughput studies, only a fraction of them were functionally annotated (**Cosmas D.Arnold, 2013; Y. E. Li et al., 2021; Yao et al., 2022**).

The proper expression of essential fate genes in different cell types is often controlled by specific enhancers (**Kvon et al., 2021; Pachano et al., 2022**). Here we have identified an intestinal enhancer for *Ctnnb1* and name it as ieCtnnb1 (intestinal enhancer of *Ctnnb1*). Reporter mice showed that ieCtnnb1 is predominantly active in the base of small intestinal crypts and across the epithelium of large intestine. Knockout of ieCtnnb1 slows down turnovers of intestinal epithelia at physiology and cancer conditions in a Wnt/β-catenin dependent manner. The human ieCTNNB1 contains a SNP that is associated with *CTNNB1* expression levels in human gastrointestinal epithelia. The enhancer activity of ieCTNNB1 in CRC tissues is higher than that in adjacent normal tissues and positively correlates with *CTNNB1* expression levels. HNF4α and phosphorylated CREB1 at serine 133 (p-S133-CREB1) were found to associate with ieCtnnb1 and regulate *Ctnnb1* transcription.

Results

ieCtnnb1 is a gastrointestinal enhancer of *Ctnnb1*

We previously identified an evolutionarily conserved upstream enhancer for *Ctnnb1* – neCtnnb1, which regulates neocortical neurogenesis (**Figure 1 - figure supplement 1A**). We reasoned that there might be other potential enhancer regions that control *Ctnnb1* expression in a cell-specific manner.

145 Therefore, we scanned upstream regions of *Ctnnb1* for active enhancer
146 properties – open chromatin with enriched H3K27ac and H3K4me1 – in
147 different tissues using data retrieved from the ENCODE database. Interestingly,
148 we noticed that a region that is 29,068 base pair (bp) upstream of the
149 transcription starting site (TSS) for *Ctnnb1* displayed typical enhancer feature
150 in intestinal tissues and resides in the same topologically associating domain
151 (TAD) with *Ctnnb1* (**Figure 1A, Figure 1 - figure supplement 2A**). The region,
152 named as ieCtnnb1 (intestinal enhancer of *Ctnnb1*), is at open chromatin status
153 (DNase I hypersensitive site) and enriched with H3K27ac and H3K4me1, two
154 histone marks for active enhancers, in 8-week-old mouse small intestine tissue
155 (**Figure 1A**). Importantly, the enrichment of H3K27ac at ieCtnnb1 is also
156 prominent in embryonic intestine and stomach tissue, as well as in adult kidney
157 and liver (**Figure 1 - figure supplement 1B and D**). In contrast, the enrichment
158 was not detected in non-gastrointestinal tissues such as embryonic and adult
159 brain (**Figure 1 - figure supplement 1D**). In line with signatures of active
160 enhancers, the enrichment of H3K4me3 and H3K36me3 at ieCtnnb1 is
161 negligible in all examined tissues (**Figure 1A, Figure 1 - figure supplement
162 1B and C**). Notably, unlike neCtnnb1, the primary sequence of ieCtnnb1 is not
163 conserved among vertebrates (**Figure 1A**, bottom).

164 We next performed *in vitro* and *in vivo* analyses to validate ieCtnnb1's
165 enhancer activity. First, the 2,153 bp core region (CR), representing the
166 H3K27ac peak region of ieCtnnb1, could drive the expression of luciferase
167 reporter in multiple cell types (**Figure 1 - figure supplement 2B**). Second, the
168 ieCtnnb1 reporter mice ($H11^{i.enh}$) were constructed by inserting the reporter
169 cassette – 5'-*Shh*'s promoter-ieCtnnb1-CR-*LacZ*-*iCre*-3' – into the *H11* locus
170 (**Figure. 1B**). Of note, the *Shh* promoter alone at the *H11* locus did not drive
171 the expression of reporter gene in all examined tissue (**Kvon et al., 2020**).
172 Wholemount β-galactosidase (β-gal) staining of 8-week-old tissues revealed
173 prominent ieCtnnb1-*LacZ* signals along the gastrointestinal (GI) tract. The

174 signal exhibited a proximal-low to distal-high gradient, with the ileum, cecum,
175 and colon showing the strongest signals (**Figure. 1B, Figure 1 - figure**
176 **supplement 2C**). The stomach and proximal duodenum also displayed
177 reporter activity driven by ieCtnnb1 (**Figure. 1B, Figure 1 - figure supplement**
178 **2C**). β-gal staining of intestinal sections revealed that the ieCtnnb1-*LacZ* signal
179 could be visualized at the bottom of small intestinal crypts and in the entire large
180 intestinal epithelia, but is absent in sections of liver, kidney, and spleen (**Figure**
181 **1 - figure supplement 2D and data not shown**). Interestingly, the proximal-
182 low to distal-high gradient of ieCtnnb1-*LacZ* signal along the small intestine
183 corresponds to the expression pattern of β-catenin (**Figure 1 - figure**
184 **supplement 2E**).

185 The transcription activity of ieCtnnb1 is strongest at the bottom of crypts,
186 where *Lgr5*-expressing CBC cells and Paneth cells (PCs) reside. To more
187 precisely elucidate cell types in which ieCtnnb1 is active, we crossed $H11^{i.enh}$
188 mice with *Lgr5*-EGFP-IRES-CreERT2 (*Lgr5*-EGFP) mice to obtain 8-week-old
189 $H11^{i.enh}$;*Lgr5-EGFP* mice. Small intestinal crypts were respectively harvested
190 from *Lgr5-EGFP* and $H11^{i.enh}$;*Lgr5-EGFP* mice followed by enrichment of both
191 eGFP+ and eGFP- cells (**Figure 1 - figure supplement 2F**). Quantitative RT-
192 PCR (RT-qPCR) analyses indicated that *LacZ* transcripts could be detected in
193 both eGFP+ and eGFP- crypt cells in $H11^{i.enh}$;*Lgr5-EGFP* mice (**Figure 1 -**
194 **figure supplement 2F**). Next, sections of $H11^{i.enh}$ crypts were subjected with
195 β-gal staining followed by immunohistochemistry of OLFM4 (a CBC marker) or
196 lysozyme (a PC marker). Data showed X-gal signals are in close proximity with
197 both OLFM4 and lysozyme (**Figure. 1C**), suggesting that the activity of
198 ieCtnnb1 is present in both CBCs and PCs.

199 We further examined the ieCtnnb1 activity in GI tracts of postnatal day 7
200 (P7) pups, when GI epithelia are rapidly expanding. The ieCtnnb1-*LacZ* signals
201 could be visualized in epithelia of P7 small and large intestines, aligning well
202 with the distribution of canonical Wnt signaling illustrated by the BAT-Gal mice

203 (**Figure 1 - figure supplement 2G and H**). Together, ieCtnnb1 drives
204 transcription in embryonic intestinal epithelia, the base of small intestinal crypts
205 and large intestinal epithelia of adult mice.
206

207 **ieCtnnb1 knockout decreased the expression of *Ctnnb1* in intestinal**
208 **epithelia**

209 We next examined whether ieCtnnb1 controls the transcription of *Ctnnb1*
210 in intestinal epithelia. For this purpose, we employed CRISPR/Cas9-mediated
211 gene editing to delete the genomic region containing ieCtnnb1 (**Figure 1 -**
212 **figure supplement 2I**). Homozygous ieCtnnb1 knockout (*Ctnnb1*$^{\Delta i.enh}$) mice
213 were born in Mendelian ratios and thrived through adulthood. Interestingly, the
214 body weight of 8-week-old male *Ctnnb1*$^{\Delta i.enh}$ mice was slightly but significantly
215 lighter than that of wild-type controls (**Figure. 1D and F**), but the length of small
216 and large intestines of *Ctnnb1*$^{\Delta i.enh}$ mice was comparable to that of control mice
217 (**Figure. 1E, G and H**). We then collected crypts from small and large intestine,
218 finding that the expression levels of *Ctnnb1* were decreased by 26.5% and 22.3%
219 respectively in *Ctnnb1*$^{\Delta i.enh}$ crypts (**Figure. 1I and J**). In contrast, the expression
220 level of *Ctnnb1* in the *Ctnnb1*$^{\Delta i.enh}$ liver remained unaltered (**Figure 1 - figure**
221 **supplement 2J**). In addition, the expression of genes located in the same TAD
222 as *Ctnnb1* and ieCtnnb1, including *Ulk4*, *Rpl14* and *Entpd3*, was not changed
223 in *Ctnnb1*$^{\Delta i.enh}$ small intestinal crypts (**Figure 1 - figure supplement 2K**). These
224 data suggest that ieCtnnb1 plays a specific role in regulating the transcription
225 of *Ctnnb1* in intestinal epithelia.

226 In epithelial tissues, most β-Catenin is localized at cell adhesion sites to
227 maintain barrier integrity, while a smaller fraction translocates into the nucleus
228 to activate transcription upon Wnt ligand binding. We therefore carried out
229 nuclear/cytosol fractionation assays, which revealed a substantial decrease in
230 the levels of both nuclear (49.5%) and cytosolic (29.8%) β-Catenin in small
231 intestinal crypts of *Ctnnb1*$^{\Delta i.enh}$ mice (**Figure. 1K and L**). RNA-seq

232 transcriptome and RT-qPCR analyses revealed a significant reduction in the
233 expressions of Wnt target genes in *Ctnnb1*$^{\Delta i.enh}$ crypts. Additionally, the gene
234 set enrichment analysis (GSEA) showed that the expression levels of many
235 components of the Wnt signaling pathway were also downregulated (**Figure.**
236 **1M and N, Figure 1 - figure supplement 3**). Together, the loss of ieCtnnb1
237 compromised the Wnt signaling in intestinal epithelia by reducing *Ctnnb1*
238 transcription.
239

240 **Loss of ieCtnnb1 altered cellular composition and expression profiles of**
241 **small intestinal crypts**

242 The canonical Wnt/β-catenin signaling is essential for the construction and
243 homeostasis of intestinal epithelia (**Mah et al., 2016**). Because ieCtnnb1
244 maintains the expression level of *Ctnnb1* of intestinal crypts, we investigated
245 how the deletion of ieCtnnb1 affects cellular components and functions of
246 intestinal crypts. We performed single-cell sequencing on EpCAM+ epithelial
247 cells from small intestinal crypts of 10-week-old *Ctnnb1*$^{\Delta i.enh}$ and control
248 (*H11*$^{i.enh}$) mice (n = 2 female mice for each genotype) (**Figure. 2A, Figure 2 -**
249 **figure supplement 1A**) (**Ayyaz et al., 2019; Huang et al., 2022**). Uniform
250 Manifold Approximation and Projection (UMAP) was employed for
251 dimensionality reduction to cluster cells, then well-established marker genes for
252 intestinal epithelial cells were mapped onto the UMAP representation to
253 designate cell types (**Haber et al., 2017; Gu et al., 2022**) (**Figure. 2B, Figure**
254 **2 - figure supplement 1B-D**). Of note, a small population of crypt cells remains
255 undefined, as we did not exclude non-epithelial cells such as immune cells,
256 erythrocytes, or endothelial cells during the enrichment of EpCAM+ epithelial
257 cells. Additionally, our focus was exclusively on epithelial cell types, and we did
258 not consider other cell types when defining cell populations (**Figure 2 - figure**
259 **supplement 1D**). First, in accordance with bulk RNA-seq and RT-qPCR results,
260 the expression levels of *Ctnnb1* were downregulated in almost all *Ctnnb1*$^{\Delta i.enh}$

261 crypt cells, and the expression of *Axin2* was decreased in CBCs and TACs
262 (**Figure. 2C and D**). Second, the proportion of PCs was decreased by 49.2%
263 in *Ctnnb1*$^{\Delta i.enh}$ crypts, which was confirmed by the immunohistochemical (IHC)
264 staining of *Defensin 5α*, a PC marker (**Figure. 2E and F**). The ieCtnnb1-driving
265 *LacZ* could be detected in the PC cluster (n = 4 10-week-old mice) (**Figure 2 -**
266 **figure supplement 1E**). Accordingly, the expression levels of examined PC
267 markers – *Lyz1*, *Pla2g2a*, *Wnt3* and *Math1* – were all significantly compromised
268 in *Ctnnb1*$^{\Delta i.enh}$ crypts (**Figure. 2G**). The number of goblet cells (GCs) was
269 slightly (not statistically significant) reduced upon loss of ieCtnnb1 (**Figure 2 -**
270 **figure supplement 1F**). Third, the proliferative capability of CSCs and TACs
271 were mildly reduced in *Ctnnb1*$^{\Delta i.enh}$ crypts, as the proportion of G2/M cells and
272 the expression of *Mki67* were decreased in the two cell types (**Figure. 2H-J**).
273 Consistently, the numbers of Ki67-positive cells and EdU-labeled cells (4 hours
274 pulse) were decreased by 16.1% and 21.9%, respectively, in *Ctnnb1*$^{\Delta i.enh}$ small
275 intestinal epithelia (**Figure. 2K and L**). Fourth, in secretory cells (PCs GCs and
276 EECs), as well as enterocytes/absorptive cells (mature enterocytes (mECs)
277 and immature enterocytes (imECs), and stem cells of *Ctnnb1*$^{\Delta i.enh}$ crypts, the
278 expression of genes related to secretory functions including *Lyz1*, *Ang4*, *Muc2*,
279 and *Mmp7* was decreased. In contrast, the expression of markers for absorptive
280 cells such as *Fabp6*, *Apoa1*, *Fabp2*, and *Reg3b* was elevated (**Figure. 2M and**
281 **N, Figure 2 - figure supplement 1G**). Accordingly, gene ontology (GO)
282 analyses showed in stem cells and secretory cells of *Ctnnb1*$^{\Delta i.enh}$ crypts,
283 upregulated genes were enriched with terms associated with absorptive
284 functions including ribosome biogenesis and oxidative phosphorylation;
285 whereas downregulated genes in stem cells and secretory cells were
286 respectively enriched with terms related to cell division and secretory functions
287 (**Figure 2 - figure supplement 1H and I**). In contrast, in mECs, downregulated
288 genes were enriched with terms associated with absorptive functions (**Figure 2**
289 **- figure supplement 1J**).

290 In summary, the loss of ieCtnnb1 results in a reduction in the number of
291 PCs, compromises stem cell proliferation, and disrupts the expression of genes
292 related to secretory and absorptive functions. These effects could be attributed
293 to a combination of reduced Wnt/β-catenin signaling and dysregulated crosstalk
294 among crypt cells.
295

296 **ieCtnnb1 deletion inhibits tumorigenesis of intestinal cancers by**
297 **suppressing Wnt/β-catenin signaling**

298 Tumorigenesis of most colorectal cancer (CRC) is associated with aberrant
299 activation of the Wnt/β-catenin signaling (**Zhu & Li, 2023**). To investigate
300 whether knockout of ieCtnnb1 could suppress the carcinogenesis of Wnt-driven
301 intestinal tumors, we crossbred *Ctnnb1*$^{\Delta i.enh}$ mice with *Apc*$^{Min/+}$ mice. In *Apc*$^{Min/+}$
302 mice, a nonsense mutation of the *Apc* gene results in the translation of
303 truncated and dysfunctional APC protein, leading to failed degradation and
304 nuclear translocation of β-catenin. *Apc*$^{Min/+}$ mice spontaneously develop
305 intestinal tumors due to enhanced canonical Wnt/β-catenin signaling in the
306 intestinal epithelia, particularly in stem cells (**Su et al., 1992**). The survival
307 period of *Ctnnb1*$^{\Delta i.enh}$;*Apc*$^{Min/+}$ mice (median survival - 255 days) was
308 significantly longer than the *Apc*$^{Min/+}$ mice (median survival - 165 days), with the
309 former having a heavier body weight (**Figure. 3A and C**). Strikingly, the
310 *Ctnnb1*$^{\Delta i.enh}$;*Apc*$^{Min/+}$ mice barely grow colorectal cancers and have much fewer
311 intestinal tumors compared to *Apc*$^{Min/+}$ mice, with significantly smaller tumor
312 area (**Figure. 3B, D-F, Figure 3 - figure supplement 1A-C**). IHC analyses
313 showed that tumors in *Ctnnb1*$^{\Delta i.enh}$;*Apc*$^{Min/+}$ large and small intestines had much
314 fewer Ki67+ proliferating cells, expressed significant less β-catenin, but
315 contained more Muc2-expressing Goblet cells, suggesting *Ctnnb1*$^{\Delta i.enh}$;*Apc*$^{Min/+}$
316 tumors behave like normal epithelia (**Figure. 3G-L, Figure 3 - figure**
317 **supplement 1D-I**). Consistently, RNA-seq transcriptome experiments showed
318 that *Ctnnb1*$^{\Delta i.enh}$;*Apc*$^{Min/+}$ colorectal cancers significantly downregulated genes

associated with the Wnt signaling pathway, pluripotency of stem cells, and gastric cancer; whereas increased expression of genes related to normal epithelial functions including oxidative phosphorylation, adhesion, protein digestion and absorption, and Mucin biosynthesis (**Figure. 3M-O**). Thus, ablation of ieCtnnb1 deters tumorigenesis of intestinal cancers by suppressing the Wnt signaling.

Human ieCTNNB1 drives the expression of reporter gene in the gastrointestinal tract

We next investigated whether the human genome also harbors an intestinal enhancer for *CTNNB1*. A region with open chromatin (DNase I hypersensitivity) and enrichment of H3K27ac/H3K4me1 was identified at 38,489 bp upstream of human *CTNNB1* in adult small intestine and colon tissues (**Figure. 4A**). Moreover, the H3K27ac enrichment is also present in esophagus but not in non-GI tissues (**Figure 4 - figure supplement 1A**). Similar to ieCtnnb1, the 3 kb-long human genomic region, named as ieCTNNB1, resides in the same TAD as the promoter of *CTNNB1* (**Figure 4 - figure supplement 1B**). We generated ieCTNNB1 reporter mice (*H11*$^{hi.enh}$) and observed that ieCTNNB1 could drive *LacZ* expression in the bottom of small intestinal crypts and the entire epithelia of large intestine, also exhibiting a proximal-low to distal-high pattern (**Figure. 4B**). Notably, the LacZ signal driven by human ieCTNNB1 was less intense than that driven by mouse ieCtnnb1, potentially attributed to species-specific TF-enhancer interactions.

The H3K27ac-enriched region of ieCTNNB1 was divided into five equal parts for the luciferase reporter assay. Experiments demonstrated that each of the five ieCTNNB1 subregions individually increased luciferase activity in both HCT116 and HeLa cells (**Figure. 4C, Figure 4 - figure supplement 1C**). We then conducted CRISPR mediated activation and interference in HCT-15 colorectal cancer cells using three guide RNAs (gRNAs) targeting ieCTNNB1,

348 which respectively enhanced and inhibited transcription of *CTNNB1* (**Figure.**
349 **4D**). Together, ieCTNNB1 is the intestinal enhancer of *CTNNB1* for human GI
350 epithelia.
351
352 **ieCTNNB1 is activated in colorectal cancer and its activity positively**
353 **correlates with the expression of *CTNNB1***
354 CRC, one of the most prevalent cancers in human, is often associated with
355 aberrant activation of the Wnt signaling (**J. Li et al., 2021**). We then studied
356 whether the occurrence of CRC is associated with enhancer activation of
357 ieCTNNB1. We previously conducted paired analyses of chromatin
358 immunoprecipitation sequencing (ChIP-seq) for H3K27ac and H3K4me3,
359 alongside RNA-seq on 68 CRC samples and their adjacent normal (native)
360 tissue (**Q. L. Li et al., 2021**). In the current study, we performed analyses for
361 the enrichment of H3K27ac and H3K4me3 at ieCTNNB1 and *CTNNB1*
362 promoter regions, as well as the expression levels of *CTNNB1*, followed by
363 combined analyses (**Figure. 5A, Figure 5 - figure supplement 1**). As
364 anticipated, the expression levels of *CTNNB1* in CRC samples were
365 significantly higher than those in neighboring native tissues (**Figure. 5B**).
366 Essentially, the enrichment of H3K27ac at ieCTNNB1 in CRC tissues were
367 significantly higher than that in native tissues (**Figure. 5C，Figure 5 - figure**
368 **supplement 1A**). In contrast, the enrichment of H3K4me3 at *CTNNB1*'s
369 promoter was comparable between cancer and native tissues (**Figure. 5C**).
370 Moreover, the enrichment of H3K27ac at ieCTNNB1 positively correlated with
371 the expression of *CTNNB1*; but the enrichment of H3K4me3 at *CTNNB1*'s
372 promoter was not associated with *CTNNB1*'s expression (**Figure. 5D**).
373 Therefore, it's the activity of enhancer but not the promoter that reflects the
374 occurrence of CRC and expression levels of *CTNNB1*.
375 By examining Genotype Tissue Expression (GTEx) eQTL data browser, a
376 single-nucleotide polymorphism (SNP) – rs15981379 (C>T) within ieCTNNB1

377 was discovered (**Figure. 5A**). Importantly, the C>T variation is inversely
378 correlated with expression levels of *CTNNB1* in the esophagus and transverse
379 colon (**Figure. 5E**). Luciferase reporter assays in HCT116 and HeLa cells
380 revealed that the C>T variation indeed compromised luciferase activity driven
381 by the ieCTNNB1-region 1 (**Figure. 5F**).
382

383 **HNF4α and p-S133-CREB1 bind to ieCTNNB1 and maintains the**
384 **expression of *CTNNB1***

385 Characterizing associated trans-factors of ieCtnnb1 and ieCTNNB1 is
386 essential for revealing related transcriptional mechanisms and holds clinical
387 relevance. By examining Cistrome Data Browser for ChIP-seq data, eight trans-
388 factors were found to associate with ieCTNNB1 in human colorectal cancer
389 cells or ieCtnnb1 in mouse GI tissues (**Figure. 6A, Figure 6 - figure**
390 **supplement 1A**). Moreover, they are relatively highly expressed and/or have
391 positive correlation with *CTNNB1*'s expression in colon cancer samples. We
392 then transduced shRNAs-expressing plasmids into HCT-15 cells to individually
393 down-regulate their expressions, revealing that decreasing the expression of
394 *CREB1* (cAMP responsive element binding protein 1) or *HNF4A* (hepatocyte
395 nuclear factor 4 alpha) could compromise *CTNNB1*'s transcription (**Figure. 6B,**
396 **Figure 6 - figure supplement 1B**). Of note, HNF4α plays crucial roles in the
397 normal development of the colon and the maintenance of epithelial barrier
398 (**Garrison et al., 2006; Cattin et al., 2009**). The phosphorylation of CREB1 at
399 serine 133 (p-S133-CREB1) is essential for its role in activation of gene
400 transcription (**Carlezon et al., 2005**). ChIP-qPCR experiments showed that
401 enrichment of p-S133-CREB1 was more prominent than CREB1 at ieCtnnb1 in
402 small intestinal crypts and at ieCTNNB1 in HCT-15 cells (**Figure. 6C and D,**
403 **Figure 6 - figure supplement 1C**). Notably, HNF4α and p-S133-CREB1 bind
404 to multiple subregions of ieCTNNB1 and ieCtnnb1, as well as the promoters of
405 *CTNNB1* and *Ctnnb1* (*pCTNNB1* and *pCtnnb1*) in HCT-15 cells and small

406 intestinal crypts (**Figure. 6C and D, Figure 6 - figure supplement 1C and D**).
407 By analyzing the GEIPA-COAD (colon adenocarcinoma) and READ (rectum
408 adenocarcinoma) database, expression levels of *CREB1* and *HNF4A* were
409 found to be significantly higher in colon and rectum cancer samples than those
410 of normal tissues (**Figure. 6E**). Furthermore, expression levels of *CREB1* and
411 *HNF4A* positively correlated with that of *CTNNB1* (**Figure. 6F**). HNF4α and p-
412 S133-CREB1 were significantly enriched at the promoter of *Ctnnb1* in *Apc*
413 mutation induced colon cancer tissues (**Figure. 6G and H**). Intriguingly,
414 knockout of ieCtnnb1 greatly diminished the association of HNF4α and p-S133-
415 CREB1 with *Ctnnb1*'s promoter (**Figure. 6G and H**). In summary, HNF4α and
416 p-S133-CREB1 were identified as essential trans-factors that bind to
417 ieCTNNB1 and maintain *CTNNB1*'s expression.
418

419 **Discussion**

420 The intestinal epithelia replenish themselves rapidly throughout lifetime,
421 which enables regeneration while predisposes to GI cancers (**Clevers, 2013**).
422 The optimal strength and dynamics of canonical Wnt/β-catenin signaling is
423 central to both homeostasis and tumorigenesis of GI tracts (**Pinto et al., 2003;**
424 **Silvia Maretto, 2003; Beumer & Clevers, 2016**). While the stabilization and
425 nuclear translocation of β-catenin is the key step for Wnt signaling activation,
426 the transcriptional control of *Ctnnb1* could be another layer of regulation (**Zhang**
427 **& Wang, 2020; Rim et al., 2022**). Here we unveiled an enhancer-dependent
428 transcriptional machinery that tunes expressions of *Ctnnb1* in multiple cell types
429 of intestinal crypts, thereby balancing homeostasis and tumorigenesis of
430 intestinal epithelia (**Figure supplement 8**).

431 Our findings reinforce the notion that the canonical Wnt signaling is
432 required for the establishment of the secretory cell lineage (**Pinto et al., 2003;**
433 **van Es et al., 2005; Pinto & Clevers, 2005**). Expression levels of markers for
434 secretory cells were greatly reduced whereas levels of markers for absorptive

435 cells were elevated in all small intestinal crypt cells of *Ctnnb1*$^{\Delta i.enh}$ mice. Fate
436 determinations of CBC daughter cells occur upon leaving the stem cell niche,
437 exposed to changing WNT, Notch and EGF levels. Progenitors losing contact
438 with PC Notch ligands upregulate DLL1 and DLL4, commit to the secretory
439 lineage, and induce Notch activity in neighboring cells, promoting enterocyte
440 differentiation (**van Es et al., 2012; Beumer & Clevers, 2020**).

441 WNT signaling not only directs PC-fated progenitors toward the crypt
442 bottom but also directly induces their differentiation (**van Es et al., 2005;**
443 **Andreu et al., 2008; Beumer & Clevers, 2020**). Single-cell sequencing and
444 reporter gene analyses indicated that the activity of ieCtnnb1 is present in PCs.
445 Knockout of ieCtnnb1 decreases number of PCs by almost 50% but the pool
446 size of CBCs was not significantly altered. A previous study showed that genetic
447 removal of PCs leads to the concomitant loss of Lgr5+ stem cells (**Sato et al.,**
448 **2011**), while other studies indicated that PCs are not mandatory niche cells for
449 the intestinal epithelia (**Garabedian et al., 1997; Durand et al., 2012; Kim et**
450 **al., 2012**). Although Wnt ligands provided by PCs may support Lgr5+ CBCs[32],
451 essential Wnt ligands are primarily supplied by subepithelial stromal
452 populations (**Degirmenci et al., 2018; Shoshkes-Carmel et al., 2018**). The
453 presence of redundancy at the stem cell niche enhances the accuracy in
454 maintaining intestinal homeostasis.

455 ieCtnnb1 knockout compromises Wnt signaling dosage, leading to PC loss,
456 dysregulation of genes controlling absorptive and secretory functions of
457 intestinal epithelia, and reduced proliferation of stem cells. These combined
458 effects could account for the lighter body weight observed in adult *Ctnnb1*$^{\Delta i.enh}$
459 mice.

460 On the other hand, colon and small intestinal tumors were rarely observed
461 in *Ctnnb1*$^{\Delta i.enh}$;*Apc*$^{Min/+}$ mice. Among the few *Ctnnb1*$^{\Delta i.enh}$ tumors analyzed,
462 they exhibited lower *Ctnnb1* expression, reduced proliferation, and behaved
463 more like normal intestinal epithelia. Different truncations or mutations of *APC*

464 lead to specific tumor types throughout the body in a Wnt/β-catenin dosage-
465 dependent manner. For example, although *Apc*^{1638N};*Ctnnb1*$^{+/-}$ mice were less
466 prone to GI cancers, *Apc*^{1638N};*Ctnnb1*$^{+/-}$ female animals tended to grow breast
467 cancers (**Bakker et al., 2013**). Therefore, the intestinal specificity of ieCtnnb1
468 makes it an ideal target to lower the strength of Wnt signaling in treating
469 colorectal cancer without affecting other tissues (**Hamdan & Johnsen, 2019;**
470 **Orouji, 2022**). Importantly, ieCTNNB1 displayed higher enhancer activity in
471 most CRC samples collected in the study. Moreover, the SNP rs15981379
472 (C>T) within ieCTNNB1 is associated with the expression of CTNNB1 in the
473 GI tract. Future population studies could investigate how the enhancer activity
474 of ieCTNNB1 and this particular SNP are associated with CRC susceptibility
475 and prognosis.

476 We noticed that after knocking out ieCtnnb1, the level of β-catenin in the
477 nuclei of small intestinal crypt cells of *Ctnnb1*$^{\Delta i.enh}$ mice decreased more
478 significantly compared to that in the cytoplasm (49.5% vs. 29.8%). Although the
479 loss of ieCtnnb1 should not directly lead to reduced nuclear translocation of β-
480 catenin, RNA-seq results showed that the loss of ieCtnnb1 causes a reduction
481 in the expression of *Bambi* (BMP and activin membrane-bound inhibitor), a
482 target gene in the canonical Wnt signaling pathway (**Figure 1M**). BAMBI
483 promotes the binding of Frizzled to Dishevelled, thereby stabilizing β-catenin
484 and facilitating its nuclear translocation (**Lin et al., 2008; Liu et al., 2014; Mai**
485 **et al., 2014; Zhang et al., 2015**). Thus, it is likely that the decreased level of
486 BAMBI resulting from the loss of ieCtnnb1 further reduced nuclear β-catenin.

487 Both mouse ieCtnnb1 and human ieCTNNB1 were able to drive reporter
488 gene expression at the base of small intestinal crypts and throughout the
489 epithelium of the large intestine. Very intriguingly, unlike the highly conserved
490 neCtnnb1 sequence among amniotes, mouse ieCtnnb1 and human ieCTNNB1
491 do not share significant homology in primary sequence (**Wang et al., 2022**).
492 Nonetheless, both ieCtnnb1 and ieCTNNB1 localize at the intergenic region 30-

493 40 kb upstream of *Ctnnb1*'s promoter. Moreover, both ieCtnnb1 and ieCTNNB1
494 contain binding motifs for HNF4α and CREB1. HNF4α and p-S133-CREB1
495 were found to associate with ieCtnnb1 and *Ctnnb1*'s promoter to maintain
496 *Ctnnb1*'s expression. These findings support the notion that conserved TF
497 binding motifs stabilize and preserve enhancer functionality over evolution
498 (**Zabidi & Stark, 2016; Wong et al., 2020**). Of note, ieCtnnb1 and ieCTNNB1
499 contain distinct TF binding motifs, which may respectively exert species-
500 specific roles in regulating the transcription of *Ctnnb1*/*CTNNB1* (**Figure 6 -**
501 **figure supplement 1E**). Future studies will dissect common and distinct
502 features of motif composition, location, order, and affinity with trans-factors
503 within ieCtnnb1 and ieCTNNB1. This analysis will provide insights how
504 sequence variations of ieCtnnb1 are adapted to intestinal homeostasis of
505 different species. Finally, it would be intriguing to explore how neocortical and
506 intestinal enhancers of *Ctnnb1* controls tissue- and stage-specific transcription,
507 as well as the existence of other potential enhancers of *Ctnnb1*.
508

509 **Methods**

510 **Mice and genotyping**

511 All animal procedures were approved by the Animal Care and Ethical
512 Committee of Medical Research Institute at Wuhan University. C57BL/6 back-
513 ground mice were housed in a temperature- and humidity- controlled
514 environment with 12-hr light/dark cycle and food/water ad libitum. *Ctnnb1*$^{\Delta i.enh}$
515 mice were generated in the Beijing Biocytogen. *H11*$^{i.enh}$ reporter mice were
516 generated in the Shanghai Model Organisms Center Inc. BAT-Gal mice were
517 provided by Dr. Jun-Lei Chang (Jackson Lab, stock number 005317). *Lgr5*-
518 EGFP-IRES-CreERT2 mice were gifts from Dr. Ye-Guang Chen (Jackson Lab,
519 stock number 008875). *APC*$^{Min/+}$ mice were gifts from Dr. Bo Zhong (Jackson
520 Lab, stock number 002020). The primer set forward 5′-atcctctgcatggtcaggtc-
521 3′/reverse 5′-cgtggcctgattcattcc-3′ was used for genotyping of BAT-Gal mice,
522 *H11*$^{i.enh}$ mice and *H11*$^{hi.enh}$ mice with a band size of 315 base pairs (bp). The
523 primer set forward 5′-gtcctgtccgtcactattatcctggc-3′/reverse5′-

524 ccactgccctgctaaagcattggt-3′/reverse 5′-tgattagttctccgggaagcccagt-3′ were
525 used for genotyping of *Ctnnb1*$^{\Delta i.enh}$ mice and band sizes for *Ctnnb1*$^{\Delta i.enh}$ mice
526 are 482 bp (wild-type allele) and 867 bp (ieCtnnb1 knockout allele). The primer
527 set forward *5′-atctcatggcaaacagacct-3′/reverse5′-tcacaaatcatctcgcaga-3′* was
528 used for genotyping of *APC*$^{Min/+}$ mice with a band size of 340 bp. The primer set
529 *forward 5′-ctgctctctgctcccagtct-3′/reverse5′-ataccccatccctttgagc-3′/reverse 5′-*
530 *gaacttcagggtcagcttgc-3′* were used for genotyping of *Lgr5*-EGFP-IRES-
531 creERT2 mice and the band sizes for 386 bp (wild-type allele) and 119 bp
532 (mutant allele).
533
534 **Cell lines**
535 HEK293T cells were gifts from Dr. Hong-Bing Shu (Wuhan University). HCT116,
536 HCT-15 and HeLa cells were purchased from the China Center for Type Culture
537 Collection. HEK293T, HeLa and HCT116 cells were grown in DMEM (Gibco)
538 supplemented with 10% fetal bovine serum (FBS) (Life Technologies) and
539 1×penicillin/streptomycin (Gibco). HCT-15 cells were maintained in RPMI-1640
540 (Gibco) containing 10% FBS (Life Technologies) and 1×penicillin/streptomycin
541 (Gibco). For routine culturing, cells were dissociated using 0.25% trypsin
542 (Gibco).
543
544 **Tissue fixation and section**
545 Intestinal and tumor tissues were dissected and cleaned in pre-cooled
546 phosphate buffered saline (PBS) and immersed in 4% paraformaldehyde (PFA)
547 overnight at 4°C. For sectioning, intestines were embedded in Tissue-Tek®
548 O.C.T. Compound (SAKURA) and cut to 8 μm thickness with a cryostat (Leica
549 CM1950).
550
551 **CRISPR/dCas9-mediated transcription activation (CRISPRa) and**
552 **interference (CRISPRi) assay**
553 CRISPRa and CRISPRi assay were performed as previously described (**Wang**
554 **et al., 2022**). In brief, SgRNAs were designed using online tool
555 (https://zlab.bio/guide-design-resources) and were listed in **Table S2**. SgRNAs
556 were cloned into lenti sgRNA (MS2)_zeo backbone vector (Addgene, #61427).

557 For CRISPRi assays, pHR-SFFV-dCas9-BFP-KRAB (Addgene, #46911) is
558 used. For CRISPRa assays, lenti MS2-P65-HSF1_Hygro (Addgene, #61426)
559 and dCAS9-VP64_GFP (Addgene, #61422) were used. To obtain lentiviral
560 particles, HEK293T cells (5 × 10^6 cells per 10-cm dish) were transiently
561 transfected with 12 μg CRISPRa or CRISPRi constructs, 6 μg psPAX2 and 6
562 μg pMD2.G. The supernatant containing lentivirus particles was harvested at
563 72 hours after transfection and filtered through Millex-GP Filter Unit (0.45 μm
564 pore size, Millipore). To obtain high virus titer, the supernatant was centrifuged
565 at 10,000×*g* for 100 minutes and concentrate to 100 μl. On the day before
566 infection, HCT-15 cells (2 × 10^5 cells per well) were inoculated in 12 well plates.
567 10 μl high titer viruses were added to each well. 72 hours after infection, cells
568 were harvested for RT-qPCR analysis.
569
570 **RNA isolation and cDNA synthesis**
571 RNAiso Plus (TAKARA) is used for RNA isolation. 1 ml RNAiso Plus was added
572 to DNase/RNase free EP tube to lyse tissues or cells, followed by adding one-
573 fifth volume of chloroform to achieve phase separation. After vigorous shaking,
574 centrifuge at 12,000×*g* for 15 minutes at 4°C. The upper aqueous phase was
575 transferred to a new DNase/RNase free EP tube and equal volume of
576 isopropanol was added to precipitate RNA. Precipitation was dissolved in
577 DNase/RNase-free water. Complementary DNAs (cDNAs) were synthesized by
578 HiScript® II Q RT SuperMix for qPCR kit (Vazyme; R222-01).
579
580 **Real-time quantitative reverse transcription PCR (RT-qPCR)**
581 cDNA was subjected to RT-qPCR using the SYBR Green assay with 2× SYBR
582 Green qPCR master mix (Bimake). PCR reactions were performed on a CFX
583 Connect Real-Time PCR Detection System (Bio-rad) under the following
584 condition: 5 minutes at 95°C, 40 cycles at 95°C for 15 seconds, 60°C for 20
585 seconds. The relative transcript level of each gene was normalized to *Gapdh*
586 (mice) or *ACTB* (human) and calculated according to the $2^{-\Delta\Delta Ct}$ method. All
587 primers used are shown in the **Table S2**.
588
589 **Isolation of murine intestinal crypt cells**

590 Murine small intestines were harvested and cut open longitudinally. After 3
591 times wash in cold PBS with Penicillin (200 U/ml) + Streptomycin (200 μg/ml)
592 (Invitrogen), small intestines were cut into 5 cm segments and incubated in pre-
593 cold PBS with 8 mM EDTA at 4°C for 2 hours. Then intestinal tissues were
594 transferred into a centrifuge tube filled with new cold PBS. Shake vigorously for
595 5 minutes and collect intestinal epithelial cells (villi plus crypts) from the
596 supernatant. Centrifuge the supernatant to collect all epithelial cells or pass
597 through 70 μm cell filter (Corning) to filter out villi. Crypts were spun down in a
598 centrifuge at 300×*g* for 5 minutes.

599

600 **Enriching *Lgr5*-EGFP$^+$ cells**

601 Crypts were collected from *Lgr5*-EGFP and *H11$^{i.enh}$*;*Lgr5*-EGFP mice, followed
602 by resuspension and single-cell digestion in DMEM containing 0.25% trypsin
603 (Gibco) at 37°C for 5 minutes. Disaggregated cells were passed through 40 μm
604 cell strainers (Corning). *Lgr5*-EGFP$^+$ and *Lgr5*-EGFP$^-$ cells were collected using
605 a BD Arial III cell sorter.

606

607 **X-Gal staining**

608 X-Gal staining is performed as described (**Wang et al., 2022**). In short, frozen
609 slides were placed in fixed buffer (0.2% PFA, 0.1 M PIPES buffer (pH 6.9), 2
610 mM MgCl2, 5 mM EGTA) for 10 minutes, followed by rinse for two times with
611 PBS containing 2 mM $MgCl_2$. Then slides were incubated with detergent
612 solution (0.1 M PBS (pH 7.3), 2 mM MgCl2, 0.01% sodium deoxycholate, 0.02%
613 Nonidet P-40) for 10 minutes. Slides were incubated with freshly prepared and
614 filtered X-Gal staining solution (0.1 M PBS (pH 7.3), 2 mM MgCl2, 0.01%
615 sodium-deoxycholate, 0.02% Nonidet P-40, 5 mM $K_3Fe(CN)_6$, 5 mM
616 $K_4Fe(CN)_6 \cdot 3H_2O$ and 1 mg/ml X-Gal) overnight in the dark at 37°C. For whole
617 gastrointestinal tissues, tissues were fixed in freshly prepared 4% PFA for 10
618 minutes, followed by rinse with detergent solution for 5 minutes by three times.
619 Tissues were incubated with freshly prepared and filtered X-Gal staining
620 solution at 37°C for a few hours.

621

622 **EdU pulse-labeling experiment**

623 Mice were intraperitoneally injected with EdU (10 mg/kg of body weight). After
624 4 hours, harvest the intestines for frozen sectioning. Staining was performed
625 using BeyoClick™ EdU Cell Promotion Kit (C0075S, Beyotime, China)
626 according to the manufacturer's manual.
627
628 **ChIP-qPCR assay**
629 Cells were cross-linked with 1% formaldehyde for 10 minutes at room
630 temperature and then quenched with 0.125 M glycine for 5 minutes and washed
631 twice with cold PBS. Cells were resuspended with 500 μl lysis buffer (50 mM
632 Tris-HCl, pH 8.0, 0.5% SDS, 5 mM EDTA) and subjected to sonication on ice
633 with an output power of 100 W, 12 minutes, 0.5 seconds on, 0.5 seconds off.
634 After centrifugation, 1% of the supernatant was taken out as input. The DNA
635 fragment lengths were measured by gel electrophoresis, showing fragments
636 between 200 bp and 500 bp, with an average length around 300 bp. The rest
637 of the sonicated lysates was diluted into 0.1% SDS and divided into several
638 equal parts. Immunoprecipitation was performed overnight at 4°C on a rotating
639 wheel with sheared chromatin, protein G agarose beads and indicated
640 antibodies: 2 μg HNF4α (Abcam, ab181604), 2 μg p-S133-CREB1 (Abcam,
641 ab32096), 2 μg IgG antibody (ABclonal, AC005). The next day, beads were
642 cleaned three times with Wash Buffer I (20 mM Tris-HCl, pH 8.0; 1% Triton X-
643 100; 2 mM EDTA; 150 mM NaCl; 0.1% SDS), Wash Buffer II (20 mM Tris-HCl,
644 pH 8.0; 1% Triton X-100; 2 mM EDTA; 500 mM NaCl; 0.1% SDS), Wash Buffer
645 III (10 mM Tris-HCl, pH 8.0; 1 mM EDTA; 0.25 M LiCl; 1% NP-40; 1%
646 deoxycholate) and TE buffer. Protein-DNA complexes were de-crosslinked in
647 120 μl elution buffer (0.1 M $NaHCO_3$, 1% SDS, 20 μg/ml proteinase K) and
648 shaken at 65°C overnight. DNA purification kit (TIANGEN) was used to extract
649 DNA fragments for qPCR.
650
651 The efficiency of qPCR primers was evaluated using gradient diluted (10^0, 10^{-1},
652 10^{-2}, 10^{-3}, 10^{-4}, 10^{-5}) of mouse or human genomes as templates. After
653 completing qPCR reaction, the dilution factors were plotted on the X-axis using
654 log10 values, and the corresponding Ct value were plotted on the Y-axis to
655 create a standard curve. The equation y = kx + b was derived, and the primer

efficiency was calculated using the formula E = 10^(-1/k) - 1. The results indicated that the primer efficiency ranged from 90% to 110%, with no significant differences observed.

Luciferase reporter assay

The luciferase reporter assay was performed as described previously (**Li et al., 2017**). Briefly, the core region of ieCtnnb1, 5 regions of ieCTNNB1 and the region containing the mutation site were respectively cloned into pGL3-promoter vector (Promega). HEK293T, HeLa and HCT116 cells were transfected with pGL3-promoter vector and the plasmids mentioned above. *Renilla* basic vector was co-transfected as a control for normalization of luciferase activity. After 48 hours of transfection, Promega Dual Glo test kit (Promega, E1910) was used to measure luciferase activity according to manufacturer's instructions.

Immunohistochemical staining

Frozen sections were dried at 37°C, fixed with 4% PFA for 10 minutes, and then washed three times with PBS. Antigen retrieval was performed using citrate buffer (pH 6, epitope retrieval solution) at 95°C for 20 minutes. Slides were then placed in 3% H_2O_2 solution for a few hours to remove endogenous catalase. After washing with PBS three times, slides were blocked with 10% normal goat serum for 1 hour, then incubated with the following primary antibodies overnight at 4°C: rabbit anti-α-defensin5 (Abcam, ab80515, 1:500), rabbit anti-Ki67 (Abcam, ab15580, 1:500), rabbit anti-β-catenin (Cell Signaling Technology, 8480T, 1:100), rabbit anti-Muc2 (Thermo Fisher Scientific, PA5-21329, 1:500). The next day, slides were incubated with biotin labeled secondary antibodies at room temperature for 1 hour. Then, slides were incubated with the avidin-biotin-peroxidase complex (VECTASTAIN Elite ABC system, Vector Labs). Finally, colorization was performed in the reaction solution (Tris-HCl (pH 7.2), 5 mg/ml 3,3'-diaminobenzidine, 0.075% H_2O_2).

H&E staining

H&E staining kit (Beyotime Biotech, C0105S) was used for experiments. Frozen

689 slides were dried at 65°C, then dripped with hematoxylin staining solution for 5
690 minutes. Excess staining solution was rinsed off with water. Slides were
691 immersed in distilled water for 5 minutes, then rinsed with 95% ethanol, and
692 stained with eosin solution for 30 seconds. Subsequently, slides were put into
693 anhydrous ethanol for 2 minutes, and cleared with xylene for 5 minutes. After
694 air dry, slides were sealed with neutral resin.

695

696 **Immunoblotting analysis**

697 Crypt cells were lysed by 1× SDS loading buffer at 95°C for 10 minutes. After
698 short centrifugation, the supernatants were loaded onto 10% SDS-
699 polyacrylamide gel electrophoresis gels. Then, proteins were transferred onto
700 polyvinylidene fluoride membrane (Millipore). Membranes were blocked with 10%
701 non-fat milk in tris-buffered saline containing 0.3% Tween 20 (TBST; pH 7.4) for
702 1 hour at room temperature. Immunoblotting was carried out used primary
703 antibody: rabbit anti-β-catenin (Cell Signaling Technology, 8480T, 1:100);
704 mouse anti-GAPDH (ABclonal, AC001, 1:1000); rabbit anti-H3 (ABclonal,
705 A2348, 1:10,000). After three times of washing with TBST, the membrane was
706 incubated with anti-rabbit immunoglobulin G (IgG)–conjugated horseradish
707 peroxidase secondary for 1 hour at room temperature. Signals were detected
708 using the ECL substrate (Thermo Fisher Scientific).

709

710 **Alcian Blue PAS Staining**

711 Alcian Blue PAS Stain Kit (Abcam, ab245876) was used for experiments. all
712 materials and prepared reagents were equilibrated to room temperature and
713 gently agitated prior to use. Tissue sections were applied with acetic acid
714 solution (3%) for 2 minutes. Then alcian blue solution (pH 2.5) was applied for
715 15-20 minutes. Slides were rinsed with running tap water for 2 minutes followed
716 by 2 changes of distilled water. Periodic acid solution was applied to tissue
717 sections for 5 minutes. After slides were rinsed with two changes of distilled
718 water, Schiff's solution was applied to tissue sections for 10-20 minutes. Slides
719 were rinsed with warm running tap water for 2 minutes followed by 2 changes
720 of distilled water. Tissue sections were applied with hematoxylin for 2 minutes.
721 Sections were rinsed in running tap water for 2 minutes followed by 2 changes

722 of distilled water. Slides were dehydrated through graded alcohols and sealed
723 with synthetic resin.
724
725 **Cell Sorting**
726 Crypt single cells were prepared as described above. Enrichment of epithelial
727 cells by cell sorting was carried out according to reported protocols with slight
728 modification (**Haber et al., 2017; Huang et al., 2022**). Cells were resuspended
729 using 1 ml PBS and stained with 5 μl anti-EpCAM-FITC (eBioScience, 11-5791-
730 82) at 4°C for 30 minutes. After washing with PBS three times, cells were
731 resuspended using 1 M FACS buffer (PBS with 1%BSA) containing 0.2 μg/ml
732 DAPI (BD Pharmingen, Cat. No. 564907). Cells were filtered with nylon
733 membrane with a 40 μm pore size. EpCAM positive cells were sorted and
734 collected based on fluorescence signals for subsequent single cell sequencing.
735 Flow cytometry data were acquired on a BD Arial III flow cytometer and
736 analyzed with FlowJo (version 10.6.2).
737
738 **Bulk RNA sequencing**
739 RNA-seq and data analyses were performed at Novogene Co., Ltd (Beijing,
740 China). Crypt cells or tumor tissues were harvested and total RNAs were
741 extracted. RNA integrity was assessed using the RNA Nano 6000 Assay Kit of
742 the Bioanalyzer 2100 system (Agilent Technologies, CA, USA). RNA-seq library
743 construction was performed as described previously (**Xu et al., 2021**). Briefly,
744 first strand cDNA was synthesized using random hexamer primer and M-MuLV
745 Reverse Transcriptase (RNase H-). Second strand cDNA synthesis was
746 subsequently performed using DNA Polymerase I and RNase H. Then, the
747 library fragments were purified with AMPure XP system (Beckman Coulter,
748 Beverly, USA). Then PCR was performed with Phusion High-Fidelity DNA
749 polymerase, Universal PCR primers and Index (X) Primer. At last, PCR
750 products were purified (AMPure XP system). The clustering of the index-coded
751 samples was performed on a cBot Cluster Generation System using TruSeq
752 PE Cluster Kit v3-cBot-HS (Illumia) according to the manufacturer's instructions.
753 After cluster generation, the library preparations were sequenced on an Illumina
754 Novaseq platform and 150 bp paired-end reads were generated.

755

756 **Bulk RNA-seq data processing**

757 For data analysis, raw data of fastq format were firstly processed through in-
758 house perl scripts. In this step, clean data were obtained by removing reads
759 containing adapter, reads containing poly-N (indicating bases that were not
760 detected and hence signal-free), and low-quality reads from the raw data. Index
761 of the reference genome was built using Hisat2 v2.0.5 and paired-end clean
762 reads were aligned to the reference genome using Hisat2 v2.0.5. featureCounts
763 v1.5.0-p3 was used to count reads numbers mapped to each gene. Differential
764 expression analysis of two groups was performed using the DESeq2 R package
765 (1.20.0). The resulting P-values were adjusted using the Benjamini and
766 Hochberg's approach for controlling the false discovery rate. Genes with an
767 adjusted P-value <0.05 found by DESeq2 were assigned as differentially
768 expressed. Gene Ontology (GO) enrichment analysis of differentially expressed
769 genes was implemented by the clusterProfiler R package, in which gene length
770 bias was corrected. clusterProfiler R package was also used to test the
771 statistical enrichment of differential expression genes in KEGG pathways. Local
772 version of the GSEA analysis tool (http://www.broadinstitute.org/gsea/index.jsp),
773 GO、KEGG、Reactome、DO and DisGeNET data sets were used for GSEA
774 independently.

775

776 **Single-Cell RNA sequencing and data analysis**

777 ScRNA-seq and data analysis were performed at Novogene Co., Ltd (Beijing,
778 China). The protoplast suspension was loaded into Chromium microfluidic
779 chips with 30 chemistry (v2 or v3) and barcoded with a 10× Chromium
780 Controller (10X Genomics). RNA from the barcoded cells was subsequently
781 reverse-transcribed and sequencing libraries constructed with reagents from a
782 Chromium Single Cell 30 v2 reagent kit (10X Genomics) according to the
783 manufacturer's instructions. Sequencing was performed with Illumina HiSeq
784 2000 according to the manufacturer's instructions. For data analysis, we use
785 FastQC to perform basic statistics on the quality of the raw reads. Raw reads
786 were demultiplexed and mapped to the reference genome by 10X Genomics
787 Cell Ranger pipeline using default parameters. All downstream single-cell

788 analyses were performed using Cell Ranger and Seurat unless mentioned
789 specifically. In brief, for each gene and each cell barcode (filtered by
790 CellRanger), unique molecule identifiers were counted to construct digital
791 expression matrices. Secondary filtration by Seurat: a gene with expression in
792 more than 3 cells was considered as expressed, and each cell was required to
793 have at least 200 expressed genes.
794
795 **Hi-C data analysis**
796 Hi-C data analysis completed by Frasergen Medicine Co., Ltd (Wuhan, China).
797 Hi-C data of BALB/c mice large intestinal epithelial cells were provided by Dr.
798 Gen Zheng (**Zheng et al., 2023**). The Hi-C data of SW480 cells was obtained
799 from deposited data (**Orouji, 2022**). According to the reported method, the
800 dynamic changes of TAD structures can be explored by calculating the relative
801 signal values of TAD boundaries. TAD boundaries that are common among
802 individuals and are not within the 2 Mb range of chromosomal ends were
803 included, followed by filtering out boundaries with interactions less than 10 in
804 the 2 Mb upstream and downstream regions. The ratio of the interaction
805 between the boundary and its 2 Mb upstream and downstream regions were
806 calculated using log2 to obtain the signal value of the TAD boundary, then the
807 minimum value was subtracted from it to finally obtain the distribution of the
808 relative signal value of each sample TAD boundary.
809
810 **ChIP-seq data analysis**
811 The human colorectal cancer patient RNA-seq FPKM files and ChIP-seq data
812 were from GEO dataset GSE156614 (**Q. L. Li et al., 2021**). All ChIP-seq raw
813 fastq data were removed of adaptor sequence. Cutadapt (version 1.16) was
814 used with the parameters -u 3 -u -10 -U 3 -U -10 -m 30. Cleaned reads were
815 aligned to the human reference genome (hg19) using bowtie2 (version 2.4.4)
816 with default settings. The CrossMap (0.6.5) package was used as a conversion
817 between different versions of the human genome (hg19 and hg38). We
818 calculated the normalized RPM (reads per million mapped reads) of ChIP-seq
819 signal at ieCTNNB1 and *CTNNB1* promoter. Briefly, reads aligned to the
820 specified region were calculated with bedtools multicov command. These reads

821 were normalized with RPM. RNA-seq data FPKM (Reads per kilobase per
822 million mapped reads) were converted to TPM (Transcript per Kilobase per
823 Million mapped reads) using R version 4.2.3.
824
825 **Knockdown experiments**
826 Target sequences for shRNAs were designed on the Merck Life Sciences
827 website (https://www.sigmaaldrich.cn) and were listed in **Table S2**.
828 Oligonucleotides for shRNAs were cloned into pLKO.1 vector (Addgene,
829 #21297). The day before transfection, HEK293T cells (2×10^5 cells per well)
830 were seeded in 12-well plates. pLKO.1 constructs, psPAX2 and pMD2.G were
831 co-transfected into HEK293T cells. After 72 hours, supernatant containing virus
832 particles was harvested and passed through Millex-GP Filter Unit (0.45 μm pore
833 size, Millipore). Viral particles were aliquoted and stored at -80°C. On the day
834 before infection, HCT-15 cells (2×10^5 cells per well) were seeded in 12-well
835 plates. 20 μl virus suspension were added to each well. After 72 hours, cells
836 were harvested for RT-qPCR to evalutate knockdown efficiency.
837
838 **Reference database**
839 ChIP-seq signals for H3K27ac, H3K4me3, H3K4me1, H3K36me3, and DNase
840 I hypersensitivity data of stomach, intestines, liver, and other tissues at different
841 stages were downloaded from the ENCODE (https://www.encodeproject.org/)
842 and their identifiers are listed in **Table S1**. In addition, ChIP-seq data for listed
843 transcription factors of cells or tissues were obtained from Cistrome Data
844 Browser (http://cistrome.org). Expressions of *HNF4A* and *CREB1* in human
845 colon (COAD) and rectal (READ) cancers were obtained from GEPIA
846 (gepia.cancer-pku.cn).
847
848 **eQTL analysis**
849 The GTEX database (https://www.gtexportal.org/home/) was used to search
850 SNPs at *CTNNB1* and the 1 MB upstream and downstream region, followed by
851 eQTL analysis. A variant, rs115981379 (C>T), was identified inside *CTNNB1*.
852 The expression levels of *CTNNB1* in 428 C/C type and 37 C/T type esophagus

853 samples, and 343 C/C type and 25 C/T type transverse colon samples were
854 also obtained in the GTEX database.
855
856 **Analyses of HNF4α and CREB1 binding motifs**
857 The JASPAR database (https://jaspar.elixir.no/) was used to analyze binding
858 motifs of HNF4α and CREB1 at ieCtnnb1/ieCTNNB1 and *Ctnnb1/CTNNB1*
859 promoter. Results are listed in **Table S3**.
860
861 **Nuclear-cytoplasmic separation**
862 Nuclear and cytoplasmic protein extraction kit (Beyotime Biotech, P0027) was
863 used for experiments. Small intestinal crypts were collected from wild-type and
864 *Ctnnb1*$^{\Delta i.enh}$ mice as described above. According to manufacturer's instructions,
865 20 μl cell precipitation was resuspended in 200 μl cytoplasmic protein extraction
866 reagent A with 1 mM PMSF. After placing on ice for 15 minutes, 10 μl
867 cytoplasmic protein extraction reagent B was added. After vigorous vortex,
868 solutions were centrifuged at 12,000×*g* for 5 minutes at 4°C. The supernatant
869 was collected as the extracted cytoplasmic protein. The precipitate was
870 resuspended with 50 μl nuclear protein extraction reagent with 1 mM PMSF.
871 Solutions were placed on ice and vortex vigorously every 2 minutes for a total
872 of 30 minutes. After centrifuging at 12,000×*g* for 10 minutes at 4°C, the
873 supernatant was collected as the extracted nuclear protein.
874
875 **Statistics**
876 All experiments reported in this study were repeated at least three independent
877 times. *In vivo* analyses were conducted with at least three animals per condition.
878 The number of animals in each experiment is depicted in Figure legends. The
879 signal intensity of tumor stain region was generated using ImageJ software
880 (version 6.0.0.260) as described previously (**Wang et al., 2021**). GraphPad
881 Prism (version 8.0.2) was used to determine statistical significance. Unpaired
882 two-tailed Student's t-test were used for analysis between two groups of equal
883 variances by *F*-tests. When the *F*-test of equal variance failed, the Welch *t*-tests
884 were used. Data comparison of three or more groups with control groups were
885 analyzed using one-way ANOVA followed by Dunnett's multiple comparison test.

886 Data comparison of three or more groups among each other were analyzed
887 using one-way ANOVA followed by Tukey's multiple comparison test. The exact
888 *P* values were reported in each figure or indicated as ****, $P < 0.0001$; ***, $P <$
889 0.001; **, $P < 0.01$; *, $P < 0.05$, ns = not significant.
890

891 **Data and code availability**

892 The GEO accession number for the bulk RNA-seq and scRNA-seq data
893 reported in this paper is GSE233979. RNA-seq data of mouse small intestinal
894 crypt and colon tumor have been deposited at GEO: GSE233977. ScRNA-seq
895 data of mouse small intestinal crypt cells in this study have been deposited at
896 GEO: GSE233978. All data are publicly available as of the date of publication.
897 Custom codes were described in detail at methods part. Any additional
898 information required to analyze the data in this paper is available from authors
899 upon reasonable request.
900

901 **References**

902 Andreu, P., Peignon, G., Slomianny, C., Taketo, M. M., Colnot, S., Robine, S., Lamarque,
903 D., Laurent-Puig, P., Perret, C., & Romagnolo, B. 2008. A genetic study of the role
904 of the Wnt/beta-catenin signalling in Paneth cell differentiation. *Dev Biol,* ***324***, 288-
905 296. https://doi.org/10.1016/j.ydbio.2008.09.027
906 Ayyaz, A., Kumar, S., Sangiorgi, B., Ghoshal, B., Gosio, J., Ouladan, S., Fink, M., Barutcu,
907 S., Trcka, D., Shen, J., Chan, K., Wrana, J. L., & Gregorieff, A. 2019. Single-cell
908 transcriptomes of the regenerating intestine reveal a revival stem cell. *Nature,* ***569***,
909 121-125. https://doi.org/10.1038/s41586-019-1154-y
910 Bakker, E. R., Hoekstra, E., Franken, P. F., Helvensteijn, W., van Deurzen, C. H., van
911 Veelen, W., Kuipers, E. J., & Smits, R. 2013. beta-Catenin signaling dosage
912 dictates tissue-specific tumor predisposition in Apc-driven cancer. *Oncogene,* ***32***,
913 4579-4585. https://doi.org/10.1038/onc.2012.449
914 Barker, N., van Es, J. H., Kuipers, J., Kujala, P., van den Born, M., Cozijnsen, M.,
915 Haegebarth, A., Korving, J., Begthel, H., Peters, P. J., & Clevers, H. 2007.
916 Identification of stem cells in small intestine and colon by marker gene Lgr5. *Nature,*
917 ***449***, 1003-1007. https://doi.org/10.1038/nature06196
918 Barreto, E. B. L., Rattes, I. C., da Costa, A. V., & Gama, P. 2022. Paneth cells and their
919 multiple functions. *Cell Biol Int,* ***46***, 701-710. https://doi.org/10.1002/cbin.11764
920 Beumer, J., & Clevers, H. 2016. Regulation and plasticity of intestinal stem cells during
921 homeostasis and regeneration. *Development,* ***143***, 3639-3649.
922 https://doi.org/10.1242/dev.133132

Beumer, J., & Clevers, H. 2020. Cell fate specification and differentiation in the adult mammalian intestine. *Nature Reviews Molecular Cell Biology,* ***22***, 39-53. https://doi.org/10.1038/s41580-020-0278-0

Carlezon, W. A., Jr., Duman, R. S., & Nestler, E. J. 2005. The many faces of CREB. *Trends Neurosci,* ***28***, 436-445. https://doi.org/10.1016/j.tins.2005.06.005

Cattin, A. L., Le Beyec, J., Barreau, F., Saint-Just, S., Houllier, A., Gonzalez, F. J., Robine, S., Pincon-Raymond, M., Cardot, P., Lacasa, M., & Ribeiro, A. 2009. Hepatocyte nuclear factor 4alpha, a key factor for homeostasis, cell architecture, and barrier function of the adult intestinal epithelium. *Mol Cell Biol,* ***29***, 6294-6308. https://doi.org/10.1128/MCB.00939-09

Cheng, X., Xu, X., Chen, D., Zhao, F., & Wang, W. 2019. Therapeutic potential of targeting the Wnt/beta-catenin signaling pathway in colorectal cancer. *Biomed Pharmacother,* ***110***, 473-481. https://doi.org/10.1016/j.biopha.2018.11.082

Chin, A. M., Hill, D. R., Aurora, M., & Spence, J. R. 2017. Morphogenesis and maturation of the embryonic and postnatal intestine. *Semin Cell Dev Biol,* ***66***, 81-93. https://doi.org/10.1016/j.semcdb.2017.01.011

Clevers, H. 2006. Wnt/beta-catenin signaling in development and disease. *Cell,* ***127***, 469-480. https://doi.org/10.1016/j.cell.2006.10.018

Clevers, H. 2013. The intestinal crypt, a prototype stem cell compartment. *Cell,* ***154***, 274-284. https://doi.org/10.1016/j.cell.2013.07.004

Clevers, H., Loh, K. M., & Nusse, R. 2014. Stem cell signaling. An integral program for tissue renewal and regeneration: Wnt signaling and stem cell control. *Science,* ***346***, 1248012. https://doi.org/10.1126/science.1248012

Clevers, H., & Nusse, R. 2012. Wnt/beta-catenin signaling and disease. *Cell,* ***149***, 1192-1205. https://doi.org/10.1016/j.cell.2012.05.012

Cosmas D.Arnold, D. G., Christoph Stelzer, Łukasz M. Boryn, Martina Rath, Alexander Stark. 2013. Genome-Wide Quantitative Enhancer Activity Maps Identified by STARR-seq. *Science,* ***339***, 1074-1077. https://doi.org/10.1126/science.1232542

Degirmenci, B., Valenta, T., Dimitrieva, S., Hausmann, G., & Basler, K. 2018. GLI1-expressing mesenchymal cells form the essential Wnt-secreting niche for colon stem cells. *Nature,* ***558***, 449-453. https://doi.org/10.1038/s41586-018-0190-3

Durand, A., Donahue, B., Peignon, G., Letourneur, F., Cagnard, N., Slomianny, C., Perret, C., Shroyer, N. F., & Romagnolo, B. 2012. Functional intestinal stem cells after Paneth cell ablation induced by the loss of transcription factor Math1 (Atoh1). *Proceedings of the National Academy of Sciences,* ***109***, 8965-8970. https://doi.org/10.1073/pnas.1201652109

Garabedian, E. M., Roberts, L. J. J., McNevin, M. S., & Gordon, J. I. 1997. Examining the Role of Paneth Cells in the Small Intestine by Lineage Ablation in Transgenic Mice. *Journal of Biological Chemistry,* ***272***, 23729-23740. https://doi.org/10.1074/jbc.272.38.23729

Garrison, W. D., Battle, M. A., Yang, C., Kaestner, K. H., Sladek, F. M., & Duncan, S. A. 2006. Hepatocyte nuclear factor 4alpha is essential for embryonic development of the mouse colon. *Gastroenterology,* ***130***, 1207-1220. https://doi.org/10.1053/j.gastro.2006.01.003

967 Gribble, F. M., & Reimann, F. 2019. Function and mechanisms of enteroendocrine cells
968 and gut hormones in metabolism. *Nature Reviews Endocrinology, **15***, 226-237.
969 https://doi.org/10.1038/s41574-019-0168-8
970 Gu, W., Wang, H., Huang, X., Kraiczy, J., Singh, P. N. P., Ng, C., Dagdeviren, S., Houghton,
971 S., Pellon-Cardenas, O., Lan, Y., Nie, Y., Zhang, J., Banerjee, K. K., Onufer, E. J.,
972 Warner, B. W., Spence, J., Scherl, E., Rafii, S., Lee, R. T., Verzi, M. P., Redmond,
973 D., Longman, R., Helin, K., Shivdasani, R. A., & Zhou, Q. 2022. SATB2 preserves
974 colon stem cell identity and mediates ileum-colon conversion via enhancer
975 remodeling. *Cell Stem Cell, **29***, 101-115 e110.
976 https://doi.org/10.1016/j.stem.2021.09.004
977 Gustafsson, J. K., & Johansson, M. E. V. 2022. The role of goblet cells and mucus in
978 intestinal homeostasis. *Nature Reviews Gastroenterology & Hepatology, **19***, 785-
979 803. https://doi.org/10.1038/s41575-022-00675-x
980 Haber, A. L., Biton, M., Rogel, N., Herbst, R. H., Shekhar, K., Smillie, C., Burgin, G., Delorey,
981 T. M., Howitt, M. R., Katz, Y., Tirosh, I., Beyaz, S., Dionne, D., Zhang, M.,
982 Raychowdhury, R., Garrett, W. S., Rozenblatt-Rosen, O., Shi, H. N., Yilmaz, O.,
983 Xavier, R. J., & Regev, A. 2017. A single-cell survey of the small intestinal
984 epithelium. *Nature, **551***, 333-339. https://doi.org/10.1038/nature24489
985 Hamdan, F. H., & Johnsen, S. A. 2019. Perturbing Enhancer Activity in Cancer Therapy.
986 *Cancers (Basel), **11***. https://doi.org/10.3390/cancers11050634
987 Huang, X.-T., Li, T., Li, T., Xing, S., Tian, J.-Z., Ding, Y.-F., Cai, S.-L., Yang, Y.-S., Wood, C.,
988 Yang, J.-S., & Yang, W.-J. 2022. Embryogenic stem cell-derived intestinal crypt
989 fission directs de novo crypt genesis. *Cell Reports, **41***.
990 https://doi.org/10.1016/j.celrep.2022.111796
991 Huels, D. J., Bruens, L., Hodder, M. C., Cammareri, P., Campbell, A. D., Ridgway, R. A.,
992 Gay, D. M., Solar-Abboud, M., Faller, W. J., Nixon, C., Zeiger, L. B., McLaughlin,
993 M. E., Morrissey, E., Winton, D. J., Snippert, H. J., van Rheenen, J., & Sansom, O.
994 J. 2018. Wnt ligands influence tumour initiation by controlling the number of
995 intestinal stem cells. *Nature Communications, **9***. https://doi.org/10.1038/s41467-
996 018-03426-2
997 Jindal, G. A., & Farley, E. K. 2021. Enhancer grammar in development, evolution, and
998 disease: dependencies and interplay. *Dev Cell, **56***, 575-587.
999 https://doi.org/10.1016/j.devcel.2021.02.016
1000 Kim, T.-H., Escudero, S., & Shivdasani, R. A. 2012. Intact function of Lgr5 receptor-
1001 expressing intestinal stem cells in the absence of Paneth cells. *Proceedings of the*
1002 *National Academy of Sciences, **109***, 3932-3937.
1003 https://doi.org/10.1073/pnas.1113890109
1004 Krausova, M., & Korinek, V. 2014. Wnt signaling in adult intestinal stem cells and cancer.
1005 *Cell Signal, **26***, 570-579. https://doi.org/10.1016/j.cellsig.2013.11.032
1006 Kurokawa, K., Hayakawa, Y., & Koike, K. 2020. Plasticity of Intestinal Epithelium: Stem
1007 Cell Niches and Regulatory Signals. *Int J Mol Sci, **22***.
1008 https://doi.org/10.3390/ijms22010357
1009 Kvon, E. Z., Waymack, R., Gad, M., & Wunderlich, Z. 2021. Enhancer redundancy in
1010 development and disease. *Nat Rev Genet, **22***, 324-336.

1011 https://doi.org/10.1038/s41576-020-00311-x
1012 Kvon, E. Z., Zhu, Y., Kelman, G., Novak, C. S., Plajzer-Frick, I., Kato, M., Garvin, T. H.,
1013 Pham, Q., Harrington, A. N., Hunter, R. D., Godoy, J., Meky, E. M., Akiyama, J. A.,
1014 Afzal, V., Tran, S., Escande, F., Gilbert-Dussardier, B., Jean-Marcais, N.,
1015 Hudaiberdiev, S., Ovcharenko, I., Dobbs, M. B., Gurnett, C. A., Manouvrier-Hanu,
1016 S., Petit, F., Visel, A., Dickel, D. E., & Pennacchio, L. A. 2020. Comprehensive In
1017 Vivo Interrogation Reveals Phenotypic Impact of Human Enhancer Variants. *Cell,*
1018 ***180***, 1262-1271 e1215. https://doi.org/10.1016/j.cell.2020.02.031
1019 Li, J., Ma, X., Chakravarti, D., Shalapour, S., & DePinho, R. A. 2021. Genetic and biological
1020 hallmarks of colorectal cancer. *GENES & DEVELOPMENT,* ***35***, 787-820.
1021 https://doi.org/10.1101/gad.348226
1022 Li, Q. L., Lin, X., Yu, Y. L., Chen, L., Hu, Q. X., Chen, M., Cao, N., Zhao, C., Wang, C. Y.,
1023 Huang, C. W., Li, L. Y., Ye, M., & Wu, M. 2021. Genome-wide profiling in colorectal
1024 cancer identifies PHF19 and TBC1D16 as oncogenic super enhancers. *Nat*
1025 *Commun,* ***12***, 6407. https://doi.org/10.1038/s41467-021-26600-5
1026 Li, Y., Wang, W., Wang, F., Wu, Q., Li, W., Zhong, X., Tian, K., Zeng, T., Gao, L., Liu, Y., Li,
1027 S., Jiang, X., Du, G., & Zhou, Y. 2017. Paired related homeobox 1 transactivates
1028 dopamine D2 receptor to maintain propagation and tumorigenicity of glioma-
1029 initiating cells. *Journal of Molecular Cell Biology,* ***9***, 302-314.
1030 https://doi.org/10.1093/jmcb/mjx017
1031 Li, Y. E., Preissl, S., Hou, X., Zhang, Z., Zhang, K., Qiu, Y., Poirion, O. B., Li, B., Chiou, J.,
1032 Liu, H., Pinto-Duarte, A., Kubo, N., Yang, X., Fang, R., Wang, X., Han, J. Y., Lucero,
1033 J., Yan, Y., Miller, M., Kuan, S., Gorkin, D., Gaulton, K. J., Shen, Y., Nunn, M.,
1034 Mukamel, E. A., Behrens, M. M., Ecker, J. R., & Ren, B. 2021. An atlas of gene
1035 regulatory elements in adult mouse cerebrum. *Nature,* ***598***, 129-136.
1036 https://doi.org/10.1038/s41586-021-03604-1
1037 Lin, Z., Gao, C., Ning, Y., He, X., Wu, W., & Chen, Y.-G. 2008. The Pseudoreceptor BMP
1038 and Activin Membrane-bound Inhibitor Positively Modulates Wnt/β-Catenin
1039 Signaling. *Journal of Biological Chemistry,* ***283***, 33053-33058.
1040 https://doi.org/10.1074/jbc.M804039200
1041 Liu, K. A. I., Song, X., Ma, H., Liu, L., Wen, X., Yu, J., Wang, L., & Hu, S. 2014. Knockdown
1042 of BAMBI inhibits β-catenin and transforming growth factor β to suppress
1043 metastasis of gastric cancer cells. *Molecular Medicine Reports,* ***10***, 874-880.
1044 https://doi.org/10.3892/mmr.2014.2305
1045 Lueschow, S. R., & McElroy, S. J. 2020. The Paneth Cell: The Curator and Defender of the
1046 Immature Small Intestine. *Front Immunol,* ***11***, 587.
1047 https://doi.org/10.3389/fimmu.2020.00587
1048 Luis, Tiago C., Naber, Brigitta A. E., Roozen, Paul P. C., Brugman, Martijn H., de Haas,
1049 Edwin F. E., Ghazvini, M., Fibbe, Willem E., van Dongen, Jacques J. M., Fodde,
1050 R., & Staal, Frank J. T. 2011. Canonical Wnt Signaling Regulates Hematopoiesis
1051 in a Dosage-Dependent Fashion. *Cell Stem Cell,* ***9***, 345-356.
1052 https://doi.org/10.1016/j.stem.2011.07.017
1053 Mah, A. T., Yan, K. S., & Kuo, C. J. 2016. Wnt pathway regulation of intestinal stem cells.
1054 *J Physiol,* ***594***, 4837-4847. https://doi.org/10.1113/JP271754

1055 Mai, Y., Zhang, Z., Yang, H., Dong, P., Chu, G., Yang, G., & Sun, S. 2014. BMP and activin
1056 membrane-bound inhibitor (BAMBI) inhibits the adipogenesis of porcine
1057 preadipocytes through Wnt/β-catenin signaling pathway. *Biochemistry and Cell*
1058 *Biology,* ***92***, 172-182. https://doi.org/10.1139/bcb-2014-0011
1059 Metcalfe, C., Kljavin, N. M., Ybarra, R., & de Sauvage, F. J. 2014. Lgr5+ stem cells are
1060 indispensable for radiation-induced intestinal regeneration. *Cell Stem Cell,* ***14***, 149-
1061 159. https://doi.org/10.1016/j.stem.2013.11.008
1062 Nakamura, T., Tsuchiya, K., & Watanabe, M. 2007. Crosstalk between Wnt and Notch
1063 signaling in intestinal epithelial cell fate decision. *J Gastroenterol,* ***42***, 705-710.
1064 https://doi.org/10.1007/s00535-007-2087-z
1065 Nalapareddy, K., Nattamai, K. J., Kumar, R. S., Karns, R., Wikenheiser-Brokamp, K. A.,
1066 Sampson, L. L., Mahe, M. M., Sundaram, N., Yacyshyn, M.-B., Yacyshyn, B.,
1067 Helmrath, M. A., Zheng, Y., & Geiger, H. 2017. Canonical Wnt Signaling
1068 Ameliorates Aging of Intestinal Stem Cells. *Cell Reports,* ***18***, 2608-2621.
1069 https://doi.org/10.1016/j.celrep.2017.02.056
1070 Noah, T. K., Donahue, B., & Shroyer, N. F. 2011. Intestinal development and differentiation.
1071 *Exp Cell Res,* ***317***, 2702-2710. https://doi.org/10.1016/j.yexcr.2011.09.006
1072 Nusse, R., & Clevers, H. 2017. Wnt/beta-Catenin Signaling, Disease, and Emerging
1073 Therapeutic Modalities. *Cell,* ***169***, 985-999.
1074 https://doi.org/10.1016/j.cell.2017.05.016
1075 Orouji, E., Raman, A. T., Singh, A. K., Sorokin, A., Arslan, E., Ghosh, A. K., Schulz, J.,
1076 Terranova, C., Jiang, S., Tang, M., Maitituoheti, M., Callahan, S. C., Barrodia, P.,
1077 Tomczak, K., Jiang, Y., Jiang, Z., Davis, J. S., Ghosh, S., Lee, H. M., Reyes-Uribe,
1078 L., … Rai, K. 2022. Chromatin state dynamics confers specific therapeutic
1079 strategies in enhancer subtypes of colorectal cancer. *Gut,* ***71(5)***, 938–949.
1080 https://doi.org/ https://doi.org/10.1136/gutjnl-2020-322835
1081 Pachano, T., Haro, E., & Rada-Iglesias, A. 2022. Enhancer-gene specificity in development
1082 and disease. *Development,* ***149***. https://doi.org/10.1242/dev.186536
1083 Pentinmikko, N., Iqbal, S., Mana, M., Andersson, S., Cognetta, A. B., Suciu, R. M., Roper,
1084 J., Luopajärvi, K., Markelin, E., Gopalakrishnan, S., Smolander, O.-P., Naranjo, S.,
1085 Saarinen, T., Juuti, A., Pietiläinen, K., Auvinen, P., Ristimäki, A., Gupta, N.,
1086 Tammela, T., Jacks, T., Sabatini, D. M., Cravatt, B. F., Yilmaz, Ö. H., & Katajisto, P.
1087 2019. Notum produced by Paneth cells attenuates regeneration of aged intestinal
1088 epithelium. *Nature,* ***571***, 398-402. https://doi.org/10.1038/s41586-019-1383-0
1089 Pinto, D., & Clevers, H. 2005. Wnt control of stem cells and differentiation in the intestinal
1090 epithelium. *Exp Cell Res,* ***306***, 357-363.
1091 https://doi.org/10.1016/j.yexcr.2005.02.022
1092 Pinto, D., Gregorieff, A., Begthel, H., & Clevers, H. 2003. Canonical Wnt signals are
1093 essential for homeostasis of the intestinal epithelium. *Genes Dev,* ***17***, 1709-1713.
1094 https://doi.org/10.1101/gad.267103
1095 Ramadan, R., van Driel, M. S., Vermeulen, L., & van Neerven, S. M. 2022. Intestinal stem
1096 cell dynamics in homeostasis and cancer. *Trends Cancer,* ***8***, 416-425.
1097 https://doi.org/10.1016/j.trecan.2022.01.011
1098 Rim, E. Y., Clevers, H., & Nusse, R. 2022. The Wnt Pathway: From Signaling Mechanisms

1099 to Synthetic Modulators. *Annu Rev Biochem,* ***91***, 571-598.
1100 https://doi.org/10.1146/annurev-biochem-040320-103615
1101 Sato, T., van Es, J. H., Snippert, H. J., Stange, D. E., Vries, R. G., van den Born, M., Barker,
1102 N., Shroyer, N. F., van de Wetering, M., & Clevers, H. 2011. Paneth cells constitute
1103 the niche for Lgr5 stem cells in intestinal crypts. *Nature,* ***469***, 415-418.
1104 https://doi.org/10.1038/nature09637
1105 Schneider, C., O'Leary, C. E., & Locksley, R. M. 2019. Regulation of immune responses
1106 by tuft cells. *Nature Reviews Immunology,* ***19***, 584-593.
1107 https://doi.org/10.1038/s41577-019-0176-x
1108 Sengupta, S., & George, R. E. 2017. Super-Enhancer-Driven Transcriptional
1109 Dependencies in Cancer. *Trends Cancer,* ***3***, 269-281.
1110 https://doi.org/10.1016/j.trecan.2017.03.006
1111 Shoshkes-Carmel, M., Wang, Y. J., Wangensteen, K. J., Tóth, B., Kondo, A., Massasa, E.
1112 E., Itzkovitz, S., & Kaestner, K. H. 2018. Subepithelial telocytes are an important
1113 source of Wnts that supports intestinal crypts. *Nature,* ***557***, 242-246.
1114 https://doi.org/10.1038/s41586-018-0084-4
1115 Silvia Maretto, M. C., Sirio Dupont, Paola Braghetta, Vania Broccoli, A. Bassim Hassan,
1116 Dino Volpin, Giorgio M. Bressan, and Stefano Piccolo. 2003. Mapping Wnt/β-
1117 catenin signaling during mouse development and in colorectal tumors. *PNAS*.
1118 Snoeck, V., Goddeeris, B., & Cox, E. 2005. The role of enterocytes in the intestinal barrier
1119 function and antigen uptake. *Microbes and Infection,* ***7***, 997-1004.
1120 https://doi.org/10.1016/j.micinf.2005.04.003
1121 Su, L. K., Kinzler, K. W., Vogelstein, B., Preisinger, A. C., Moser, A. R., Luongo, C., Gould,
1122 K. A., & Dove, W. F. 1992. Multiple intestinal neoplasia caused by a mutation in the
1123 murine homolog of the APC gene. *Science,* ***256***, 668-670.
1124 https://doi.org/10.1126/science.1350108
1125 Terrin, L., Agostini, M., Ruvoletto, M., Martini, A., Pucciarelli, S., Bedin, C., Nitti, D., &
1126 Pontisso, P. 2017. SerpinB3 upregulates the Cyclooxygenase-2 / beta-Catenin
1127 positive loop in colorectal cancer. *Oncotarget,* ***8***, 15732-15743.
1128 https://doi.org/10.18632/oncotarget.14997
1129 Tian, H., Biehs, B., Warming, S., Leong, K. G., Rangell, L., Klein, O. D., & de Sauvage, F.
1130 J. 2011. A reserve stem cell population in small intestine renders Lgr5-positive cells
1131 dispensable. *Nature,* ***478***, 255-259. https://doi.org/10.1038/nature10408
1132 van der Flier, L. G., & Clevers, H. 2009. Stem cells, self-renewal, and differentiation in the
1133 intestinal epithelium. *Annu Rev Physiol,* ***71***, 241-260.
1134 https://doi.org/10.1146/annurev.physiol.010908.163145
1135 van Es, J. H., Jay, P., Gregorieff, A., van Gijn, M. E., Jonkheer, S., Hatzis, P., Thiele, A.,
1136 van den Born, M., Begthel, H., Brabletz, T., Taketo, M. M., & Clevers, H. 2005. Wnt
1137 signalling induces maturation of Paneth cells in intestinal crypts. *Nat Cell Biol,* ***7***,
1138 381-386. https://doi.org/10.1038/ncb1240
1139 van Es, J. H., Sato, T., van de Wetering, M., Lyubimova, A., Yee Nee, A. N., Gregorieff, A.,
1140 Sasaki, N., Zeinstra, L., van den Born, M., Korving, J., Martens, A. C. M., Barker,
1141 N., van Oudenaarden, A., & Clevers, H. 2012. Dll1+ secretory progenitor cells
1142 revert to stem cells upon crypt damage. *Nat Cell Biol,* ***14***, 1099-1104.

https://doi.org/10.1038/ncb2581

Wang, A., Wang, J., Tian, K., Huo, D., Ye, H., Li, S., Zhao, C., Zhang, B., Zheng, Y., Xu, L., Hua, X., Wang, K., Wu, Q. F., Wu, X., Zeng, T., Liu, Y., & Zhou, Y. 2021. An epigenetic circuit controls neurogenic programs during neocortex development. *Development, **148***. https://doi.org/10.1242/dev.199772

Wang, J., Wang, A., Tian, K., Hua, X., Zhang, B., Zheng, Y., Kong, X., Li, W., Xu, L., Wang, J., Li, Z., Liu, Y., & Zhou, Y. 2022. A Ctnnb1 enhancer regulates neocortical neurogenesis by controlling the abundance of intermediate progenitors. *Cell Discov, **8***, 74. https://doi.org/10.1038/s41421-022-00421-2

Wong, E. S., Zheng, D., Tan, S. Z., Bower, N. L., Garside, V., Vanwalleghem, G., Gaiti, F., Scott, E., Hogan, B. M., Kikuchi, K., McGlinn, E., Francois, M., & Degnan, B. M. 2020. Deep conservation of the enhancer regulatory code in animals. *Science, **370***. https://doi.org/10.1126/science.aax8137

Xu, L., Zheng, Y., Li, X., Wang, A., Huo, D., Li, Q., Wang, S., Luo, Z., Liu, Y., Xu, F., Wu, X., Wu, M., & Zhou, Y. 2021. Abnormal neocortex arealization and Sotos-like syndrome–associated behavior in Setd2 mutant mice. *Science Advances, **7***, 1180. https://doi.org/10.1126/sciadv.aba1180

Yan, K. S., Chia, L. A., Li, X., Ootani, A., Su, J., Lee, J. Y., Su, N., Luo, Y., Heilshorn, S. C., Amieva, M. R., Sangiorgi, E., Capecchi, M. R., & Kuo, C. J. 2012. The intestinal stem cell markers Bmi1 and Lgr5 identify two functionally distinct populations. *Proc Natl Acad Sci U S A, **109***, 466-471. https://doi.org/10.1073/pnas.1118857109

Yao, L., Liang, J., Ozer, A., Leung, A. K.-Y., Lis, J. T., & Yu, H. 2022. A comparison of experimental assays and analytical methods for genome-wide identification of active enhancers. *Nature Biotechnology, **40***, 1056-1065. https://doi.org/10.1038/s41587-022-01211-7

Zabidi, M. A., & Stark, A. 2016. Regulatory Enhancer-Core-Promoter Communication via Transcription Factors and Cofactors. *Trends Genet, **32***, 801-814. https://doi.org/10.1016/j.tig.2016.10.003

Zhang, Q., Shi, X.-E., Song, C., Sun, S., Yang, G., & Li, X. 2015. BAMBI Promotes C2C12 Myogenic Differentiation by Enhancing Wnt/β-Catenin Signaling. *International Journal of Molecular Sciences, **16***, 17734-17745. https://doi.org/10.3390/ijms160817734

Zhang, Y., & Wang, X. 2020. Targeting the Wnt/beta-catenin signaling pathway in cancer. *J Hematol Oncol, **13***, 165. https://doi.org/10.1186/s13045-020-00990-3

Zhao, H., Ming, T., Tang, S., Ren, S., Yang, H., Liu, M., Tao, Q., & Xu, H. 2022. Wnt signaling in colorectal cancer: pathogenic role and therapeutic target. *Mol Cancer, **21***, 144. https://doi.org/10.1186/s12943-022-01616-7

Zheng, G., Pang, S., Wang, J., Wang, F., Wang, Q., Yang, L., Ji, M., Xie, D., Zhu, S., Chen, Y., Zhou, Y., Higgins, G. A., Wiley, J. W., Hou, X., & Lin, R. 2023. Glucocorticoid receptor-mediated Nr1d1 chromatin circadian misalignment in stress-induced irritable bowel syndrome. *iScience, **26***, 107137. https://doi.org/10.1016/j.isci.2023.107137

Zhu, Y., & Li, X. 2023. Advances of Wnt Signalling Pathway in Colorectal Cancer. *Cells, **12***. https://doi.org/10.3390/cells12030447

Acknowledgments

We thank Dr. Yeguang Chen for providing the *Lgr5*-EGFP-IRES-CreERT2 mice. We thank the Core Facility and the Animal Facility of Medical Research Institute of Wuhan University for technical support. We thank all Zhou lab members for critical reading of the manuscript. Y. Zhou was supported by grants from National Key R&D Program of China (2022YFA0806603 and 2018YFA0800700), National Natural Science Foundation of China (32270876 and 31970770), and the Fundamental Research Funds for the Central Universities (2042022dx0003 and 2042023kf0234). Y.L. was supported by grants from National Key R&D Program of China (2018YFA0800700 and 2022YFA0806603), National Natural Science Foundation of China (31970676), and Hubei Natural Science Foundation (2022CFB128).

Author contributions

Y.Z. conceived and designed the study; X.H. and J.W. performed experiments and analyzed data; C.Z. assisted with processing ChIP-seq data; J.T. and X.P. retrieved and analyzed eQTL data. M.Y. and M.W. provided RNA-seq and ChIP-seq data of colorectal cancer samples; G.Z. provided Hi-C data; Y.Z. and X.H. wrote the paper. Y.Z. and Y.L. provided funding and supervised the study. All authors discussed results and commented to the manuscript.

Competing interests

The authors claimed that they have no competing interests.

1212 **Figures**

1213

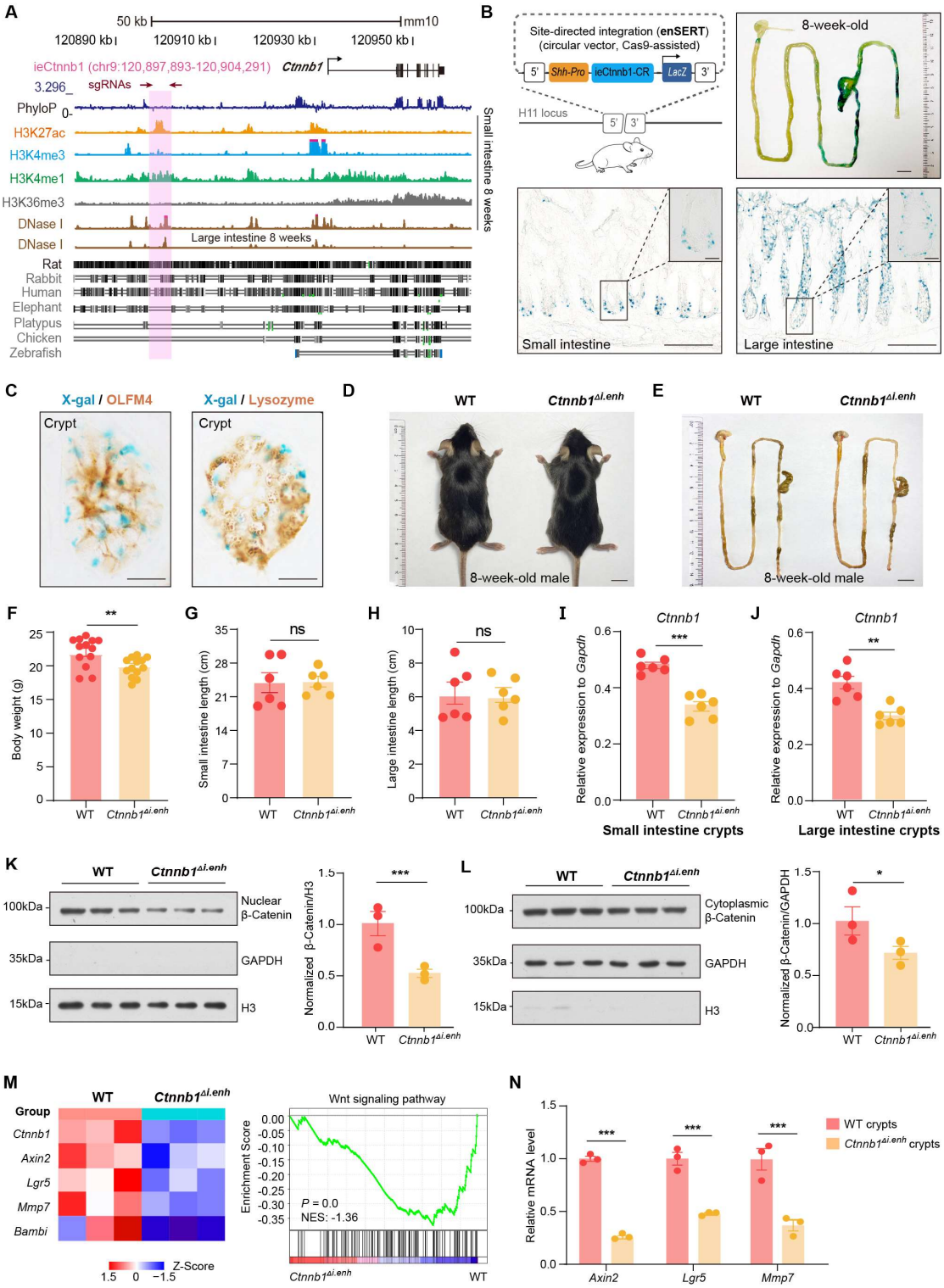

1214

1215 **Figure 1. ieCtnnb1 is an intestinal enhancer of *Ctnnb1*.** (A) Schematic

1216 representation of the upstream region of mouse *Ctnnb1* gene and the location

1217 of ieCtnnb1 (6,399 bp, pink shading), which is marked by H3K27ac and

1218 H3K4me1 peaks, and DNase I hypersensitivity in small intestine and large
1219 intestine of 8-week-old mice. The sequence conservation of the indicated
1220 species is shown at the bottom as vertical lines. Data were obtained from
1221 ENCODE. Locations of single-guide RNAs (sgRNAs) for generating ieCtnnb1
1222 knockout mice were marked. (B) Top left: a schematic illustration showing that
1223 the knock-in reporter construct carries the *Shh* promoter, ieCtnnb1 core region
1224 sequences (2,153 bp) and the *LacZ* reporter gene. Top right: X-Gal staining
1225 (blue) of the gastrointestinal (GI) tract of an 8-week-old $H11^{i.enh}$ mouse. Bottom:
1226 X-Gal staining (blue) of the small intestine (left) and colon (right) of an 8-week-
1227 old $H11^{i.enh}$ mouse. Boxed areas were enlarged at top-right corners. (C)
1228 Representative images of small intestinal crypts co-labelled by X-gal with
1229 OLFM4 (left), and X-gal with Lysozyme (right). (D-E) Representative images of
1230 whole body (d) and GIs (e) of 8-week-old male wildtype (WT) and $Ctnnb1^{\Delta i.enh}$
1231 mice. (F) Comparison of the body weight of 8-week-old male WT (n = 13) and
1232 $Ctnnb1^{\Delta i.enh}$ (n = 13) mice. (G-H) Measurements of small (G) and large (H)
1233 intestine length of 8-week-old male WT (n = 6) and $Ctnnb1^{\Delta i.enh}$ (n = 6) mice. (I-
1234 J) Relative mRNA levels of *Ctnnb1* in small (I) and large (J) intestinal crypts of
1235 WT (n = 6) and $Ctnnb1^{\Delta i.enh}$ (n = 6) mice. (K-L) Left: immunoblotting of nuclear
1236 (K) and cytoplasmic (L) β-Catenin, GAPDH and H3 of small intestinal crypts of
1237 WT (n = 3) and $Ctnnb1^{\Delta i.enh}$ (n = 3) mice. Right: histograms showing protein
1238 levels of β-Catenin normalized to H3 (K) or GAPDH (L) levels. Values of WT
1239 were set as '1'. (M) Heat map of indicated Wnt target genes and GSEA analysis
1240 of Wnt signaling pathway according to transcriptome profiles of small intestinal
1241 crypts of WT (n = 3) and $Ctnnb1^{\Delta i.enh}$ (n = 3) mice. (N) RT-qPCR showing relative
1242 mRNA levels of indicated Wnt target genes (*Axin2, Lgr5* and *Mmp7*) in small
1243 intestinal crypts of WT (n = 3) and $Ctnnb1^{\Delta i.enh}$ (n = 3) mice. Scale bars, 1 cm
1244 (B, top; D and E), 100 μm (B, bottom), 10 μm (B, magnified views; C).
1245 Quantification data are shown as means ± SEM, statistical significance was
1246 determined using an unpaired two-tailed Student's *t*-test (F-L). Quantification

1247 data are shown means ± SD, statistical significance was determined using
1248 Multiple *t*-tests - one per row (N). *$P < 0.05$, **$P < 0.01$, ***$P < 0.001$, and ****P
1249 < 0.0001. ns, not significant. NES: Normalized Enrichment Score.
1250
1251
1252

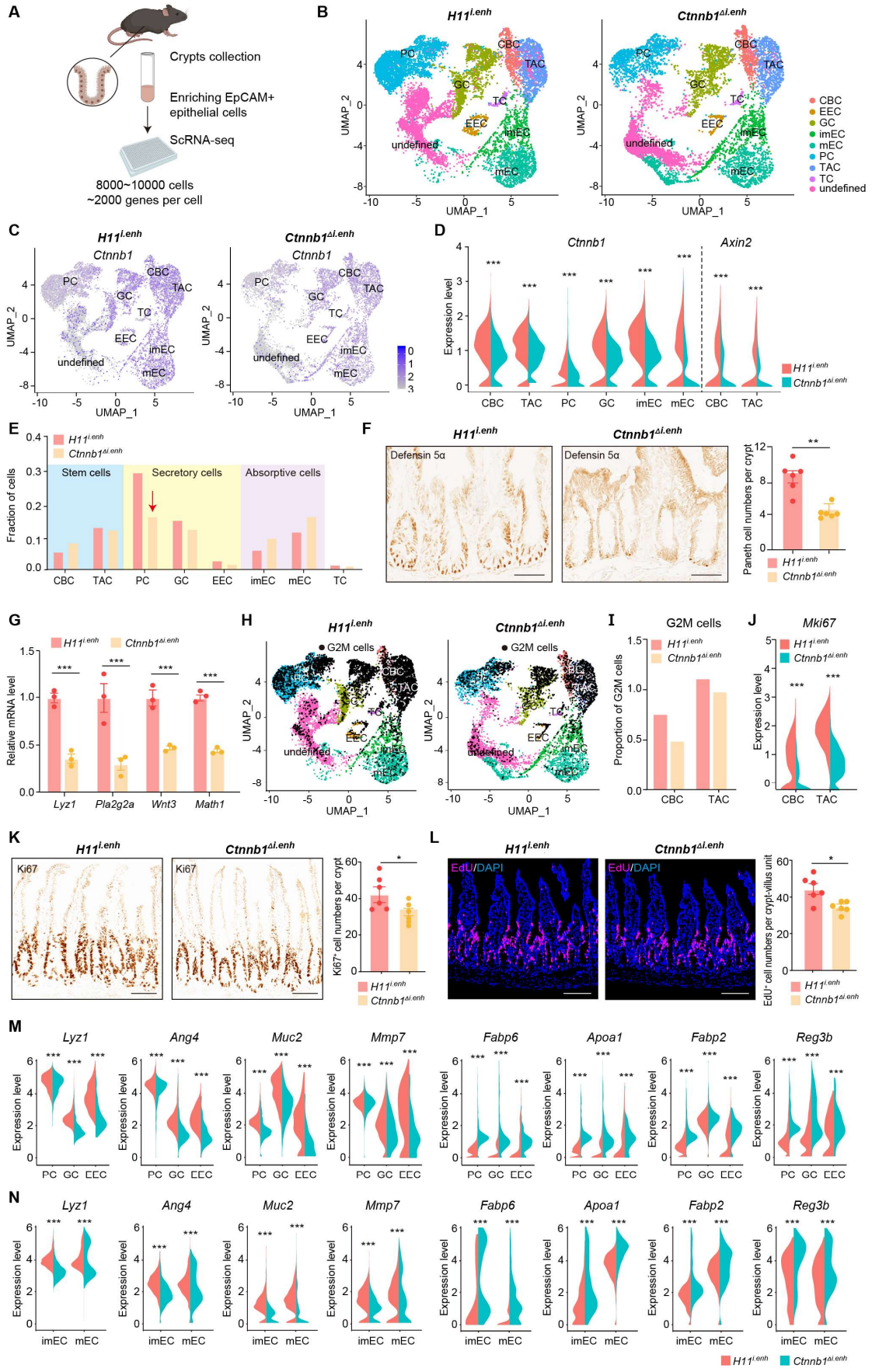

Figure 2. ieCtnnb1 knockout altered cellular composition and expression

1255 **profiles of small intestinal crypts.** (A) Schematic illustration of single-cell
1256 sequencing. Crypts were extracted from small intestines followed by
1257 fluorescence activated cell sorting (FACS) to enrich EpCAM+DAPI- epithelial
1258 cells. Cells of two 10-week-old female mice for each genotype were pooled
1259 together to perform single cell transcriptome analyses. (B) UMAP were used to
1260 visualize the clustering of 11,824 single cells from *H11*$^{i.enh}$ mice and 8,094
1261 single cells from *Ctnnb1*$^{\Delta i.enh}$ mice. Cell types were assigned according to
1262 expressions of marker genes. CBC, crypt base columnar cell; TAC, transit
1263 amplifying cell; EEC, enteroendocrine cell; imEC, immature enterocytes; mEC,
1264 mature enterocytes; GC, goblet cell; PC, Paneth cell; TC, tuft cell. (C)
1265 Expression and distribution of *Ctnnb1* in small intestinal crypt cells of *H11*$^{i.enh}$
1266 and *Ctnnb1*$^{\Delta i.enh}$ mice. (D) Violin plots showing the expression of *Ctnnb1* in CBC,
1267 TAC, PC, GC, imEC, mEC; and the expression of *Axin2* in CBC and TAC, of
1268 *H11*$^{i.enh}$ and *Ctnnb1*$^{\Delta i.enh}$ mice. (E) Comparison of the proportion of indicated small
1269 intestinal crypt cell types in *H11*$^{i.enh}$ and *Ctnnb1*$^{\Delta i.enh}$ mice. (F)
1270 Immunohistochemistry (left and middle) and quantification (right) of PCs in
1271 small intestines of *H11*$^{i.enh}$ (n = 6) and *Ctnnb1*$^{\Delta i.enh}$ (n = 6) mice. (G) RT-qPCR
1272 showing relative mRNA levels of PC marker genes (*Lyz1, Pla2g2a, Wnt3,*
1273 *Math1*) in small intestinal crypts of *H11*$^{i.enh}$ (n = 3) and *Ctnnb1*$^{\Delta i.enh}$ (n = 3) mice.
1274 (H) Distribution of G2M cells in *H11*$^{i.enh}$ and *Ctnnb1*$^{\Delta i.enh}$ small intestinal crypts,
1275 based on the expression of cell cycle marker gene *Mki67*. (I) Comparison of the
1276 proportion of G2M cells in CBC and TAC of *H11*$^{i.enh}$ and *Ctnnb1*$^{\Delta i.enh}$ small
1277 intestinal crypts. (J) Violin plots showing the expression of *Mki67* in CBC and
1278 TAC of *H11*$^{i.enh}$ and *Ctnnb1*$^{\Delta i.enh}$ small intestinal crypts. (K)
1279 Immunohistochemistry (left and middle) and quantification (right) of Ki67+ cells
1280 in small intestines of *H11*$^{i.enh}$ (n = 6) and *Ctnnb1*$^{\Delta i.enh}$ (n = 6) mice. (L)
1281 Immunofluorescence (left and middle) and quantification (right) of EdU+ cells
1282 (red) in small intestines of *H11*$^{i.enh}$ (n = 6) and *Ctnnb1*$^{\Delta i.enh}$ (n = 6) mice after 4
1283 hours EdU injection. Nuclei were labeled with DAPI (blue). (M-N) Violin plots
1284 showing expressions of marker genes for secretory cells (*Lyz1, Ang4, Muc2,*
1285 *Mmp7*) and absorptive cells (*Fabp6, Apoa1, Fabp2, Reg3b*) in secretory(M) and
1286 absorptive lineages (N) of *H11*$^{i.enh}$ and *Ctnnb1*$^{\Delta i.enh}$ small intestinal crypts. Scale
1287 bars, 50 μm (F, K, and L). Quantification data are shown as means ± SEM,

statistical significance was determined using an unpaired two-tailed Student's *t*-test (D, F, J, K, L, M and N). Quantification data are shown means ± SD, statistical significance was determined using Multiple *t*-tests - one per row (G). *$P < 0.05$, **$P < 0.01$, ***$P < 0.001$, and ****$P < 0.0001$. ns, not significant.

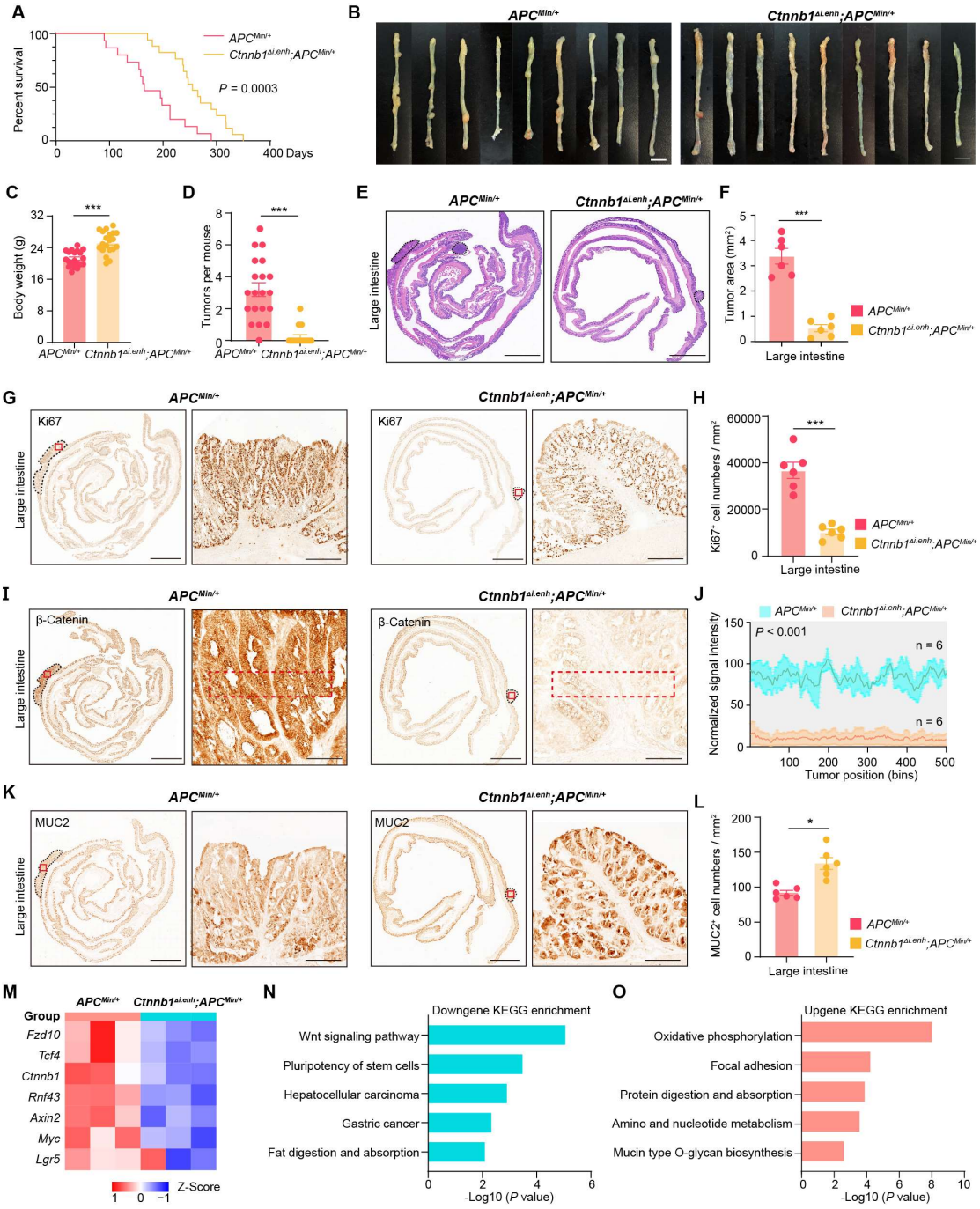

Figure 3. Knocking out ieCtnnb1 inhibits tumorigenesis of colorectal cancer. (A) Survival of *Apc*$^{Min/+}$ (n = 15) and *Ctnnb1*$^{\Delta i.enh}$;*Apc*$^{Min/+}$ (n = 17) mice. (B) Colon images of 5-month-old *Apc*$^{Min/+}$ (n = 9) and *Ctnnb1*$^{\Delta i.enh}$;*Apc*$^{Min/+}$ (n = 9) mice. (C) Weight statistics of 5-month-old *Apc*$^{Min/+}$ (n = 20) and *Ctnnb1*$^{\Delta i.enh}$;*Apc*$^{Min/+}$ (n = 20) mice. (D) The statistical analysis of tumor counts

in colons of 5-month-old *Apc*$^{Min/+}$ (n = 9) and *Ctnnb1*$^{\Delta i.enh}$;*Apc*$^{Min/+}$ (n = 9) mice. (E) Representative H&E staining images of colon sections of 5-month-old *Apc*$^{Min/+}$ and *Ctnnb1*$^{\Delta i.enh}$;*Apc*$^{Min/+}$ mice. (F) The statistical analysis of colon tumor area in 5-month-old *Apc*$^{Min/+}$ (n = 6) and *Ctnnb1*$^{\Delta i.enh}$;*Apc*$^{Min/+}$ (n = 6) mice. (G-H) Immunohistochemistry (G) and quantification (H) of Ki67+ cells in colon tumors of 5-month-old *Apc*$^{Min/+}$ (n = 6) and *Ctnnb1*$^{\Delta i.enh}$;*Apc*$^{Min/+}$ (n = 6) mice. (I-J) Immunohistochemistry (I) and signal intensity statistics (J, red dashed boxes of I) of β-Catenin in colon tumors of 5-month-old *Apc*$^{Min/+}$ (n = 6) and *Ctnnb1*$^{\Delta i.enh}$;*Apc*$^{Min/+}$ (n = 6) mice. (K-L) Immunohistochemistry (K) and quantification (L) of MUC2+ cells in colon tumors of 5-month-old *Apc*$^{Min/+}$ (n = 6) and *Ctnnb1*$^{\Delta i.enh}$;*Apc*$^{Min/+}$ (n = 6) mice. (M) The heat map showing relative expressions of Wnt signaling pathway genes of colon tumors from 5-month-old *Apc*$^{Min/+}$ (n = 3) and *Ctnnb1*$^{\Delta i.enh}$;*Apc*$^{Min/+}$ (n = 3) mice. (N-O) KEGG analyses of downregulated (N) and upregulated (O) genes in colon tumors of 5-month-old *Apc*$^{Min/+}$ (n = 3) and *Ctnnb1*$^{\Delta i.enh}$;*Apc*$^{Min/+}$ (n = 3) mice. Scale bars, 1 cm (B), 4 mm (E, G, I and K), 200 μm (magnified views in G and K), 100 μm (magnified views in I). Quantification data are shown as means ± SEM, statistical significance was determined using an unpaired two-tailed Student's *t*-test (C, D, F, H, J and L) or log-rank analysis (A). *$P < 0.05$, **$P < 0.01$, ***$P < 0.001$, and ****$P < 0.0001$. ns, not significant.

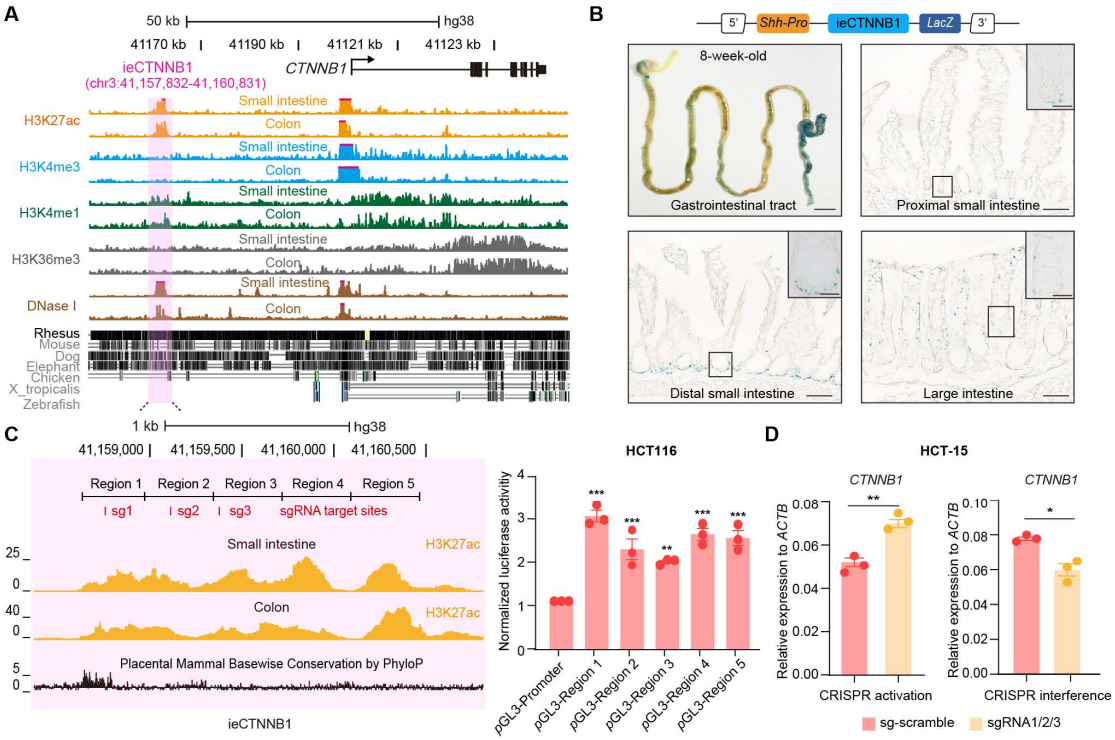

Figure 4. ieCTNNB1 is the intestinal enhancer of human *CTNNB1*. (A) Schematic representation of human *CTNNB1* gene and the location of ieCTNNB1 (3,000 bp, pink shading), which is marked by H3K27ac and H3K4me1 peaks, and DNase Ⅰ hypersensitivity in human small intestine (30-year-old female) and colon (34-year-old male). Data were obtained from ENCODE. (B) Top: a schematic illustration showing that the knock-in construct containing the *Shh* promoter, ieCTNNB1 sequences (3,000 bp), and the LacZ reporter gene. Bottom: X-Gal staining (blue) of the gastrointestinal tract, and sections of the proximal small intestine, distal small intestine, and large intestine in 8-week-old *H11*$^{hi.enh}$ mice. (C) Left: ieCTNNB1 is marked by enrichment of H3K27ac in human small intestine (30-year-old female) and colon (34-year-old male). Data were obtained from ENCODE. Locations of sgRNA target sites were indicated. Five subregions of ieCTNNB1 were shown. Right: luciferase reporter assay in HCT116 cells transfected with indicated plasmids for 48 hours. (D) RT-qPCR showing relative mRNA levels of *CTNNB1* in HCT-15 cells transfected with indicated CRISPR activation or CRISPR interference vectors for 48 hours. Scale bars, 1 cm (whole mount in B), 100 μm (sections in B), 10

1340 μm (magnified views in B). Quantification data are shown as means ± SEM,
1341 statistical significance was determined using one-way ANOVA analysis (C) and
1342 an unpaired two-tailed Student's *t*-test (D). *$P < 0.05$, **$P < 0.01$, ***$P < 0.001$,
1343 and ****$P < 0.0001$. ns, not significant.
1344

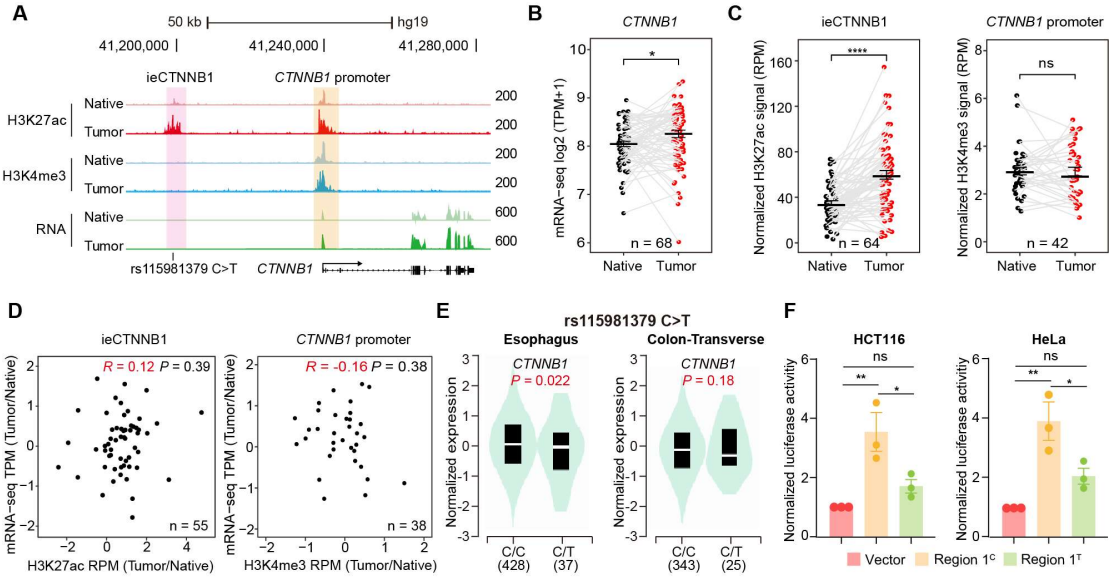

Figure 5. ieCTNNB1 is activated in colorectal cancer and its activity positively correlates with the expression of *CTNNB1*. (A) Schematic representation of ieCTNNB1 (pink shading) and *CTNNB1* promoter (yellow shading), which is respectively marked by H3K27ac and H3K4me3 peaks, and mRNA signals in native and tumor tissues of a patient with colorectal cancer. The location of risk mutation site was indicated. (B) Comparison of *CTNNB1* expression levels in native and tumor tissues of colorectal cancer patients (n = 68). (C) Left: comparison of H3K27ac signals at ieCTNNB1 in native and tumor tissues of colorectal cancer patients (n = 64). Right: comparison of H3K4me3 signals at *CTNNB1* promoter in native and tumor tissues of colorectal cancer patients (n = 42). (D) Left: correlation between H3K27ac signals at ieCTNNB1 and *CTNNB1* expression in native and tumor tissues of colorectal cancer patients (n = 55). Right: correlation between H3K4me3 signals at *CTNNB1* promoter and *CTNNB1* expression in native and tumor tissues of colorectal cancer patients (n = 38). (E) Left: comparison of *CTNNB1* expression in esophagus between subjects with common sequence (C/C, n = 428) and variant sequence (C/T, n = 37). Right: comparison of *CTNNB1* expression in transverse colon between subjects with common sequence (C/C, n = 343) and variant sequence (C/T, n = 25). (F) Luciferase reporter assay in HCT116 and

1365 HeLa cells transfected with indicated plasmids for 48 hours. Quantification data
1366 are shown as means ± SEM, statistical significance was determined using a
1367 paired (B, C and D) or unpaired (E) two-tailed Student's *t*-test and Two-way
1368 ANOVA analysis (F). *$P < 0.05$, **$P < 0.01$, ***$P < 0.001$, and ****$P < 0.0001$.
1369 ns, not significant. R: Pearson correlation.
1370

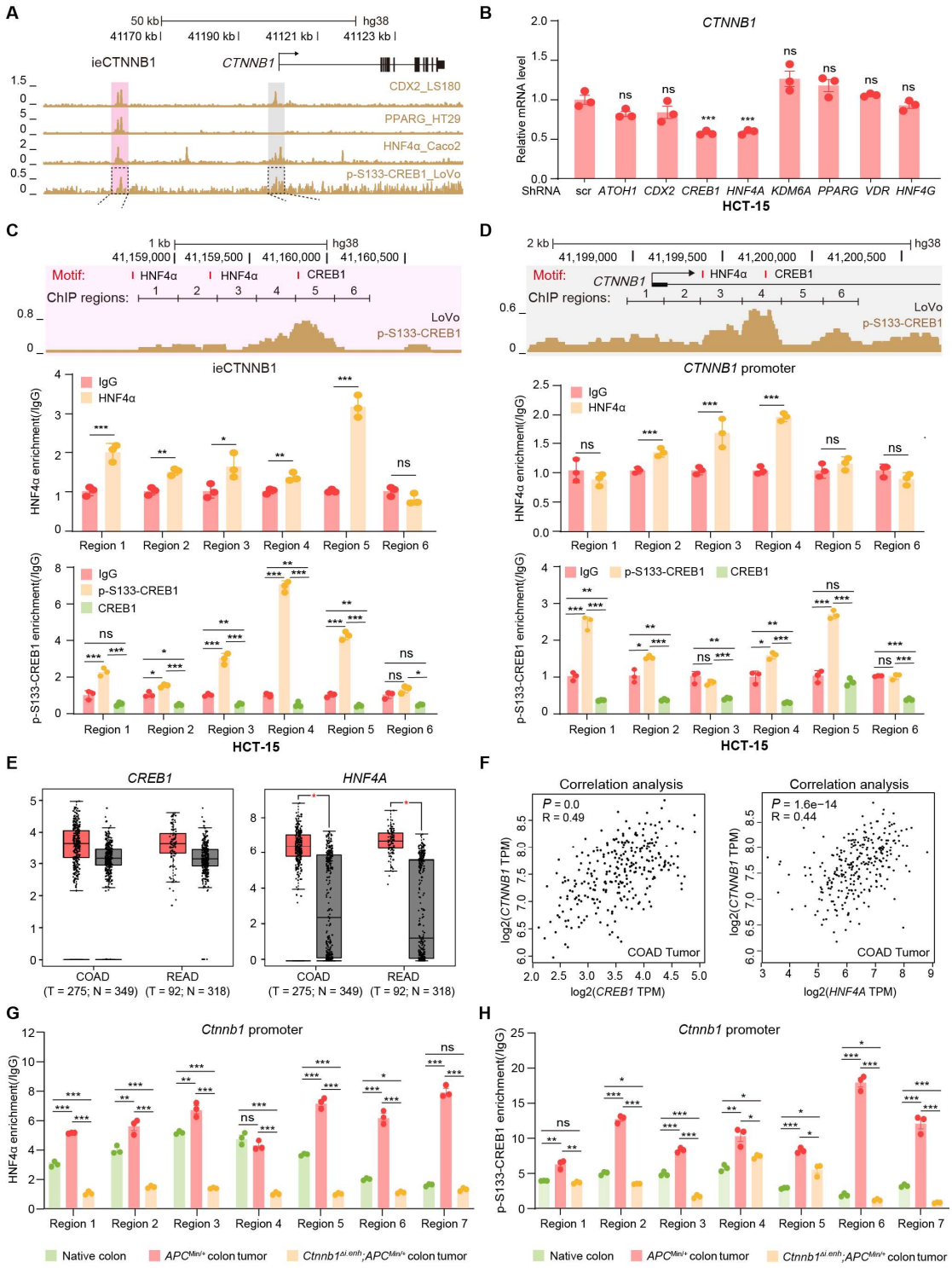

Figure 6. HNF4*α* and p-S133-CREB1 associate with ieCTNNB1 to regulate *CTNNB1*'s transcription. (A) ChIP-seq tracks of indicated trans-acting factors enriched at ieCTNNB1 (pink shading) and *CTNNB1* promoter (grey shading) in indicated colorectal cancer cell lines. Shaded regions were enlarged in C (pink) and D (grey) respectively. (B) RT-qPCR showing relative mRNA levels of

1377 *CTNNB1* in HCT-15 cells transfected with indicated shRNA-expressing
1378 plasmids for 48 hours. The expression level of *CTNNB1* in cells transfected with
1379 scramble (scr) shRNA was set to '1'. (C-D) Top: schematic diagram showing
1380 the enrichment of p-S133-CREB1 at ieCTNNB1 (C) and *CTNNB1*'s promoter
1381 (D). Locations of HNF4α and CREB1 binding motif sites were indicated. Middle
1382 and bottom: ChIP-qPCR showing enrichment of HNF4α (middle), CREB1 and
1383 p-S133-CREB1 (bottom) at ieCTNNB1 (C) and *CTNNB1*'s promoter (D) in HCT-
1384 15 cells. Locations of ChIP regions were indicated. (E) Comparison of
1385 expression levels of *CREB1* and *HNF4A* between native and tumor tissues in
1386 colon adenocarcinoma (COAD) and rectum adenocarcinoma (READ) tumors.
1387 (F) Correlations between the expression level of *CTNNB1* and those of *CREB1*
1388 or *HNF4A* in COAD tumors. (G-H) ChIP-qPCR showing enrichment of HNF4α
1389 (G) and p-S133-CREB1 (H) at *Ctnnb1* promoter in native colon tissues of WT
1390 (n= 3) mice, tumor tissues of $Apc^{Min/+}$ (n= 3) mice and $Ctnnb1^{\Delta i.enh}$;$Apc^{Min/+}$ (n= 3)
1391 mice. Quantification data are shown as means ± SEM, statistical significance
1392 was determined using one-way ANOVA analysis (B), unpaired two-tailed
1393 Student's *t*-test (E and F) and Multiple *t*-tests - one per row (C, D, G and H). *P
1394 < 0.05, **P < 0.01, ***P < 0.001, and ****P < 0.0001. ns, not significant. R:
1395 Pearson correlation.
1396